Ab Initio Approaches to Nuclear Structure

Robert Roth

Abstract Ab initio nuclear structure theory has experienced a phase of ground-breaking developments over the past decade. Compared to the situation in the early 2000s, we now have a rich variety of powerful and complementary tools that connect the underlying theory of the strong interaction to nuclear structure observables. This enables us to describe a much larger domain of nuclei and observables with controlled and quantified theoretical uncertainties—in the ab initio spirit. In this lecture we provide a pedagogical introduction into the ab initio toolbox with a focus on basis-expansion approaches, particularly on configuration interaction methods, like the no-core shell model, and decoupling approaches, like the in-medium similarity renormalization group.

1 Introduction

The landscape of methods that define the state-of-the-art in ab initio nuclear structure theory has been completely transformed since the early 2000s. New and innovative many-body schemes have been developed that radically expand the boundaries of what is possible computationally. At the same time, the connection to the underlying theory of the strong interaction has be strengthened through the use of effective field theories for the construction of nuclear interactions.

In this lecture we provide an introduction to ab initio nuclear structure theory with a focus on basis-expansion methods. This is really meant to be a lecture and not a review article. We will present the material in a pedagogical manner, focussing on systematics, clarity, and consistency. We will explore the basic theoretical concepts and their interrelations and not so much the multitude of applications and results. We

Robert Roth

Institut für Kernphysik, Technische Universität Darmstadt, Schlossgartenstr. 2, 64289 Darmstadt;
Helmholtz Forschungsakademie Hessen für FAIR, Schlossgartenstr. 9, 64289 Darmstadt, Germany
e-mail: robert.roth@physik.tu-darmstadt.de

will not attempt to cover the field of ab initio theory completely—given the wealth of recent developments this would fill a complete volume of this lecture series.

2 The Big Picture

We start by formulating the general nuclear structure problem as a quantum many-body problem. Already the first steps in this formulation imply specific assumptions, e.g., on the effective degrees-of-freedom for the theoretical description. This, in turn, has consequences for the formulation of the relevant interactions and, thus, the effective Hamiltonian governing the structure and dynamics of the system. Finally, the quantum many-body problem has to be solved, which in our case amounts to the solution of a many-particle Schrödinger equation. In this section, we go through these steps and establish the basic language and notation. We will also give an overview of the different classes of approaches to the many-body problem and address the meaning of the term 'ab initio'.

Constituents. We consider nuclei as quantum multi-particle systems, composed of nucleons as effective degrees of freedom. It is understood that nucleons themselves have a complicated substructure, being bound states of quarks governed by the complicated quark-gluon interactions of Quantum Chromodynamics (QCD). However, we do not wish to resolve this underlying layer of microphysics.

This seemingly obvious choice (from the perspective of low-energy nuclear structure physics) has profound consequences. From the beginning we decide to work with an *effective theory* that has a limited range of validity resulting from the choice of the effective degrees of freedom. By construction the nucleons in our effective theory are point-like particles, they are inert and have no internal structure. This is obviously not the full truth—nucleons are extended objects with a typical root-mean-square radius of their charge distribution (for the proton) of around 0.8 fm and they have internal excitations, e.g. the Δ resonances at about 300 MeV of excitation energy. For the effective theory of point-nucleons this implies: (i) a limited range of applicability and (ii) the need to account for corrections to the relevant observables.

In a proper effective theory, these points should follow in a systematic and transparent fashion from the formulation of the theory. The range of validity should be clearly defined from the outset and the theory should provide a consistent way to construct the corrections to observables resulting from the unresolved physics. One of the significant advances in nuclear structure theory over the past decade addresses exactly this point—with the advent of chiral effective field theory, the step from QCD to the world of point-nucleons has become a well-defined procedure. Nuclear structure calculations have matured from a model to an effective theory.

Interactions. The simplifications with respect to the degrees of freedom necessarily entail complications with respect to the interactions among them. The effective interaction of point-nucleons also has to encapsulate the complicated quark-gluon dynamics at the level of QCD that is not resolved in our description. The dynamics of

quarks and gluons creates the net interaction that two or more nucleons experience and this net effect has to be mimicked by the effective interaction among point-nucleons in the effective theory.

This situation is not unique to nuclear structure physics. We find a similar scenario in molecular physics when describing a system of atoms. Consider, e.g., a system of two or more neutral ^{4}He atoms. A simple effective theory could assume point-like ^{4}He particles, not resolving the complicated internal structure of the atoms. The effective interaction between the point-atoms has to capture all the underlying dynamics of the atoms, this is the famous van der Waals interaction in atomic and molecular physics. The mechanism behind these forces can be understood intuitively. At large distances the electrically neutral atoms do not affect each other and there is no interaction. Only at short distances, the mutual polarization of their electron distributions induces a net interaction. A similar mechanism is at work when color-neutral baryons come close enough so that their quark-gluon distributions overlap.

In atomic physics it is possible to compute the residual interaction among the atoms from solving the Schrödinger equation for the multi-electron two-atom problem. In principle this can also be done in QCD, specifically in Lattice QCD simulations. Research along these lines is on the way [1, 2, 3] and has shown how difficult this problem is. For the time being, we have to resort to effective field theories based on QCD for a description of the nuclear interaction [4]. Chiral effective field theories (EFT) have become a foundation of modern nuclear structure theory.

Many-Body Problem. Having defined the constituents and their interactions, we are now in the position to formulate the basic equation that governs the structure and dynamics of the many-body system, the Schrödinger equation. At this point we restrict ourselves to a non-relativistic description of the many-body problem—relativistic effects might enter as specific corrections in the Hamiltonian, but we will not attempt a fully relativistic treatment.

In most cases we are interested in stationary properties of nuclei and we do not need to address the explicit time evolution of the many-body problem. Thus, the central equation we have to deal with is the stationary Schrödinger equation, in other words, the eigenvalue problem of the Hamiltonian

$$\hat{H} \ket{\Psi_n} = E_n \ket{\Psi_n} , \tag{1}$$

where $\hat{H}$ is the Hamiltonian of the A-nucleon system, E_n are the energy eigenvalues, and $\ket{\Psi_n}$ are the corresponding eigenvectors. We will use the representation-independent Dirac notation throughout this lecture. The discrete index $n = 0, 1, 2, ...$ already implies that we are concerned with the discrete part of the spectrum of the Hamiltonian, i.e., the bound states of the nucleus. We will not discuss the continuous part of the spectrum, i.e., the domain of nuclear scattering, reactions and resonances in this lecture.

For a more detailed look at the eigenvalue problem, we first have to define the Hilbert space in which we are working. We consider a system of A indistinguishable nucleons with spin and isospin degrees of freedom. A typical basis for the description of the single-nucleon degrees of freedom in a finite nucleus consists of a spatial part,

which encodes position and momentum information, a spin part and an isospin part. For the spin part, we simply use the eigenstates of the the single-particle spin operators $\hat{\mathbf{s}}$ and $\hat{s}_z$ with quantum numbers $s = \frac{1}{2}$ and $m_s = \pm\frac{1}{2}$. Analogously for the isospin, we use eigenstates of $\hat{\mathbf{t}}$ and $\hat{t}_3$ with quantum numbers $t = \frac{1}{2}$ and $m_t = \pm\frac{1}{2}$. For this lecture we will limit ourselves to spherical basis sets $|nlm_l\rangle$ in the spatial degrees of freedom, labeled by a generic radial quantum number n and orbital angular momentum quantum numbers l and m_l. We will couple orbital angular momentum and spin to obtain total angular momentum quantum numbers j and m. The coupled single-particle states thus read

$$|p\rangle = |nljmm_t\rangle = |n(l\tfrac{1}{2})jm\rangle \otimes |\tfrac{1}{2}m_t\rangle \ . \tag{2}$$

We will use the collective indices $p, q, \ldots$ to label single-particle basis states throughout this lecture.

When proceeding to the many-body system, we have to take the permutation antisymmetry of the states for a system of identical fermions into account. The simplest way to construct a basis of the A-body antisymmetric Hilbert space $\mathcal{H}_A$ uses antisymmetrized product states—so-called Slater determinants. Starting from a complete single-particle basis $\{|p\rangle\}$, we select A different single-particle states $|p_1\rangle, \ldots, |p_A\rangle$ and construct product states for all possible permutations of the single-particle indices. Summing over all these permutations with appropriate signs defines an *antisymmetrized product state* or *Slater determinant*:

$$|p_1...p_A\rangle = \frac{1}{\sqrt{A!}} \sum_\pi \mathrm{sgn}(\pi)\hat{P}_\pi |p_1\rangle \otimes \ldots \otimes |p_A\rangle \ . \tag{3}$$

Here, $\hat{P}_\pi$ is the permutation operator, which rearranges the single-particle indices according to the permutation π, and $\mathrm{sgn}(\pi)$ indicates the signum or parity of the permutation π. The pre-factor is chosen such that the many-body states are normalized provided that the single-particle states are normalized. Note that our notation does not explicitly indicate the antisymmetric character of the A-body states $|p_1...p_A\rangle$— antisymmetry is always implied and we will never go back to simple product states.

The set of all antisymmetrized product states generated from an orthonormal single-particle basis automatically provides an orthonormal basis of the antisymmetric A-nucleon Hilbert space $\mathcal{H}_A$. This is very convenient.

Another very convenient aspect of this basis is the formalism of second quantization. We can define creation operators $\hat{a}_p^\dagger$ and annihilation operators $\hat{a}_p$ that add or remove particles to or from a given Slater determinant $|p_1...p_A\rangle$, automatically yielding a normalized antisymmetrized $(A+1)$ or $(A-1)$-particle state, respectively. We can even construct a complete A-body Slater determinant starting from the zero-body vacuum state $|0\rangle$ through the application of a chain of creation operators:

$$|p_1...p_A\rangle = \hat{a}_{p_1}^\dagger \cdots \hat{a}_{p_A}^\dagger |0\rangle \ . \tag{4}$$

The complications of antisymmetry are now hidden in the anti-commutation relations of fermionic creation and annihilation operators. Finally, creation and annihilation

operators can be used to represent any operator, e.g., the components of the Hamiltonian, in an elegant way—we will make heavy use of this later on.

Basis Expansion, Truncation, Convergence. Why did we go through these basic elements from many-body quantum mechanics? Well, they prompt a simple and powerful strategy for the solution of the many-body Schrödinger equation. This strategy can be summarized under the label *basis expansion* and is at the heart of all methods discussed in this lecture.

Assume we have constructed an orthonormal basis $|\Phi_\nu\rangle$ of the A-nucleon Hilbert space $\mathcal{H}_A$, e.g., the antisymmetrized product states $|\Phi_\nu\rangle = |\{p_1...p_A\}_\nu\rangle$ discussed before. We can immediately use this basis to transfer the abstract, representation-independent eigenvalue problem (1) into a specific representation in the $|\Phi_\nu\rangle$ basis. We can expand the eigenstates $|\Psi_n\rangle$ in this basis

$$|\Psi_n\rangle = \sum_\nu C_\nu^{(n)} |\Phi_\nu\rangle \tag{5}$$

with expansion coefficients $C_\nu^{(n)}$. Furthermore, we can multiply eq. (1) from the left with all possible basis vectors $\langle\Phi_\nu|$ and insert the above expansion of the eigenstates to obtain a coupled system of algebraic equations

$$\sum_{\nu'} \langle\Phi_\nu| \hat{H} |\Phi_{\nu'}\rangle C_{\nu'}^{(n)} = E_n C_\nu^{(n)} \qquad \forall \nu , \tag{6}$$

which can be conveniently cast into a matrix equation

$$\begin{pmatrix} \langle\Phi_1| \hat{H} |\Phi_1\rangle & \langle\Phi_1| \hat{H} |\Phi_2\rangle & \langle\Phi_1| \hat{H} |\Phi_3\rangle & \cdots \\ \langle\Phi_2| \hat{H} |\Phi_1\rangle & \langle\Phi_2| \hat{H} |\Phi_2\rangle & \langle\Phi_2| \hat{H} |\Phi_3\rangle & \cdots \\ \langle\Phi_3| \hat{H} |\Phi_1\rangle & \langle\Phi_3| \hat{H} |\Phi_2\rangle & \langle\Phi_3| \hat{H} |\Phi_3\rangle & \cdots \\ \vdots & \vdots & \vdots & \ddots \end{pmatrix} \cdot \begin{pmatrix} C_1^{(n)} \\ C_2^{(n)} \\ C_3^{(n)} \\ \vdots \end{pmatrix} = E_n \begin{pmatrix} C_1^{(n)} \\ C_2^{(n)} \\ C_3^{(n)} \\ \vdots \end{pmatrix} . \tag{7}$$

So the Schrödinger equation or the abstract eigenvalue problem of the Hamiltonian translates naturally into a standard matrix eigenvalue problem. The input for this are the many-body matrix elements of the Hamiltonian $\langle\Phi_\nu| \hat{H} |\Phi_{\nu'}\rangle$ in the basis of choice, and the output are the energy eigenvalues E_n and the eigenvectors $(C_1^{(n)}, C_2^{(n)}, C_3^{(n)}, ...)^{\mathrm{T}}$, which contain the expansion coefficients.

Seems like a pretty straightforward numerical exercise to solve this eigenvalue problem. The only problem is that the matrix is infinite dimensional. Already the single-particle basis $|p\rangle$ and the single-nucleon Hilbert space $\mathcal{H}_1$ are infinite dimensional, and the A-nucleon basis $|p_1...p_A\rangle$ and the A-nucleon Hilbert space are even more so.

The way out of this misery are *truncations*. We discard many-body basis states based on a specific truncation criterion and, in this way, reduce the infinite-dimensional basis to a finite set of states. This finite set spans the so-called *model space* $\mathcal{M}_A$, which is a sub-space of $\mathcal{H}_A$. There are many ways to define physics-motivated truncation criteria, and we will dive into this in Sect. 5.1. For the time

being and as a simple example, assume that the single-particle basis $|p\rangle$ is truncated to a finite set—in case $|p\rangle$ is built from a harmonic-oscillator basis, we could simply limit the principal oscillator quantum number $e = 2n + l \leq e_{\max}$ with the truncation parameter $e_{\max}$ and discard all single-particle states with $e > e_{\max}$. This renders the A-body basis finite and defines the full configuration interaction scheme, as discussed later.

Imposing a basis truncation implies a departure from the exact solution of (1). The solution of the eigenvalue problem in the finite model space is only an approximation to the exact Schrödinger equation. However, it is a very controlled approximation, since the full problem and the exact solution are formally recovered if we include more and more states into the model space and effectively remove the truncation again, i.e., if we consider $e_{\max} \to \infty$ and thus $\mathcal{M}_A \to \mathcal{H}_A$. Obviously, we cannot do this in practical calculations, but we can explore the dependence of the solution and of all observables on the truncation. Ideally we would observe *convergence*, i.e., the observables becoming independent of the truncation for sufficiently large truncation parameters and model spaces. Whether or not we are able to reach convergence before the matrix is getting intractably large will be a central question for later.

Conclusions—Ab Initio. So far, we have approached nuclear structure theory from a bird's-eye view. However, we have already encountered the key concepts and difficulties of many nuclear structure methods: basis choice, model-space truncation, convergence, uncertainty quantification. We have seen enough to discuss the notorious qualifier 'ab initio' that is used as a quality label for many recent nuclear structure calculations. There is no agreed-upon definition of what qualifies a method as ab initio, and we will not attempt to provide a rigorous definition. However, we will mention some aspects relevant for the use of the term.

First, none of the nuclear structure methods qualifies as 'ab initio' or 'from first principles' from the perspective of QCD—there are promising attempts to describe light nuclei in lattice QCD [1, 2, 3], but more work is needed to provide quantitative results. The baseline for the many-body solutions are Hamiltonians rooted in QCD, but using nucleons as effective degrees of freedom. Today, chiral EFT provides the most systematic way to establish the connection to QCD. However, the chiral EFT construction of interactions in itself uses truncations and ad-hoc assumptions, which affect the nuclear observables. Furthermore, chiral EFT interactions come with parameters, the low-energy constants, that have to be fitted to experimental data. The selection of data and the experimental uncertainties of the data itself influence the predicted nuclear observables as well.

Second, all methods for the solution of the many-body problem contain some level of approximation. For basis-expansion methods the truncation to a finite model space introduces such an approximation, and there might be additional truncations and approximations involved. These truncations affect the observables and, therefore, necessitate a systematic convergence analysis. The many-body method has to provide systematic control parameters that govern the transition to a formally exact solution—for basis-expansion methods this is the transition from the model space to the full Hilbert space. We have to use these control parameters to demonstrate

that observables are sufficiently converged, i.e., sufficiently independent of the truncation. Doing this is not straightforward, particularly if multiple truncations and approximations are involved—the convergence with respect to all of them has to be addressed, otherwise the calculation is merely an uncontrolled approximation.

Third, the truncations and approximations introduced at the level of the Hamiltonian and in the many-body solution are the source of systematic theory uncertainties. Even though we strive for convergence with respect to all truncations, we will hardly ever reach complete convergence. Therefore, the remaining systematic uncertainties in the theoretical predictions have to be quantified. This uncertainty quantification should be done within the theoretical framework used for the calculation, e.g., by exploring the convergence behavior with respect to truncations and by translating this into an uncertainty estimate for each and every observable. In addition, there might be statistical uncertainties inherited from experimental data used to calibrate the theory, e.g., for the fit of the low-energy constants in the interaction. Some many-body methods also produce additional statistical uncertainties through some statistical sampling process. For a long time nuclear theory has been (and often still is) remarkably unconcerned about its uncertainties—a complete discussion of all sources of uncertainties leading to qualified error bars (not just guesswork) should be part of all ab initio calculations. If not, the label 'ab initio' is not justified.

3 Hamiltonian

The foundation of any ab initio calculation is the Hamiltonian $\hat{H}$. As discussed in the previous section, it is not trivial to write down the Hamiltonian for the nuclear many-body problem. We have to develop an effective theory framework to construct the interactions that enter into the Hamiltonian—this theory framework will be chiral EFT. Before addressing this, we start with a discussion of the symmetries of the Hamiltonian and the consequences for the many-body eigenstates.

3.1 Intrinsic Hamiltonian

Nuclei are self-bound systems. Unlike the electrons in an atom that are trapped in the Coulomb field of the central nucleus, the nucleons are held together solely by their mutual interactions. This seemingly trivial fact already has important consequences, it implies a number of symmetries.

From the fact that all the relevant interactions are intrinsic, i.e., act only among the nucleons of the system, we can conclude that the properties of the nucleus, e.g., the binding or excitation energies, are invariant under basic spatial transformations. These energies must not change if we place the nucleus at a different position in space, or rotate the nucleus as a whole, or give the nucleus a non-vanishing total momentum. Therefore, we expect the Hamiltonian to exhibit these symmetries as

well: translational invariance, rotational invariance, and invariance under momentum boosts, i.e., the Galilean symmetries.

For the construction of the operators for the two- and multi-nucleon interactions ($\hat{V}_{NN}$, $\hat{V}_{3N}$, etc.) these symmetries are taken into account explicitly. In addition, we have to pay attention to the kinetic energy operator $\hat{T}$. Naively, we might write the kinetic energy in the A-body system as a sum of single-nucleon kinetic energy operators

$$\hat{T} = \sum_{i=1}^{A} \frac{1}{2m} \hat{\mathbf{p}}_i^2 \, , \tag{8}$$

where m is the average nucleon mass—in most ab initio calculations the mass difference between proton and neutron is not included. This operator is not invariant under momentum boosts, it contains the kinetic energy associated with the center-of-mass motion of the nucleus. We have to subtract the operator for the center-of-mass kinetic energy $\hat{T}_{cm}$ to arrive at the so-called *intrinsic kinetic energy*

$$\hat{T}_{int} = \hat{T} - \hat{T}_{cm} = \sum_{i=1}^{A} \frac{1}{2m} \hat{\mathbf{p}}_i^2 - \frac{1}{2Am} \left(\sum_{i=1}^{A} \hat{\mathbf{p}}_i \right)^2$$
$$= \sum_{i<j}^{A} \frac{1}{2m} (\hat{\mathbf{p}}_i - \hat{\mathbf{p}}_j)^2 = \sum_{i=1}^{A} \frac{1}{2m(A-1)} \hat{\mathbf{p}}_i^2 + \sum_{i<j}^{A} \frac{1}{2m} \hat{\mathbf{p}}_i \cdot \hat{\mathbf{p}}_j \, . \tag{9}$$

The last two expressions show two practical forms of the intrinsic kinetic energy that are being used in nuclear structure calculations—they are equivalent at the operator level. However, within an approximate many-body scheme, the results obtained with the two forms might differ [5].

With this we obtain the so-called *intrinsic Hamiltonian*, which obeys all the Galilean symmetries:

$$\hat{H} = \hat{T}_{int} + \hat{V}_{NN} + \hat{V}_{3N} + \cdots \, . \tag{10}$$

All the many-body approaches discussed in the following will use this type of Hamiltonian. However, this does not guarantee that the solutions and observables in a truncated many-body calculation also exhibit these symmetries. We will come back to this point.

3.2 Practitioners view on chiral EFT

For constructing the two- and many-nucleon interaction operators, most ab initio approaches resort to chiral EFT. There are many excellent reviews on chiral EFT for nuclear interactions [6, 7, 8, 9, 10, 11, 12], and we invite the reader to explore these sources.

We will look at chiral EFT from the perspective of a user, i.e., a many-body practitioner that needs interactions as input for the solution of the many-body problem.

Even from this vantage point, there are important aspects in the fabric of chiral EFT we need to be aware of:

- *Chiral order*: Chiral EFT is built on an expansion in a small parameter and the organization of contributions in powers of this small parameter, which is called power counting. The small parameter Q is a ratio of the typical momentum scale in the system P and the breakdown-scale of the EFT Λ_χ and is of the order $Q = P/\Lambda_\chi \approx 1/3$. The expansion of the interaction is truncated at some finite power in Q. We will call this the *chiral order* and consider interactions at leading-order (LO) corresponding to Q^0, next-to leading oder (NLO) with Q^2, next-to-next-to leading order (N^{2}LO) with Q^3, and so on.
- *Many-body forces*: Starting from N^{2}LO, chiral EFT predicts contributions that correspond to irreducible three-nucleon (3N) interactions. Starting from N^{3}LO irreducible four-nucleon interactions emerge. The fact that these many-body forces emerge at higher orders in the expansion indicates that they are expected to be successively weaker. It is a great success of chiral EFT that these terms emerge naturally, in a systematic fashion and in a coherent theoretical framework.
- *Regulator scheme and scale*: Present chiral EFT interactions use a cutoff regularization of divergencies, which is implemented though momentum-dependent cutoff functions. Different types of momenta in the two- and few-nucleon system can be used to formulate the regulators functions (relative momenta vs. momentum transfer). We can even formulate cutoff functions in coordinate space or hybrid schemes that use different regulators for different terms. In addition to the regulator scheme, the cutoff scale Λ can be chosen in a certain range.
- *Fitting strategy*: For given chiral order, regulator scheme and scale, a number of low-energy constants (LECs) associated with the contact terms have to be determined, typically by a fit to experimental data. There are different strategies to approach this parameter fit. One option is to fix all LECs that appear at the level of two-body interactions in the two-body system, all additional LECs that appear in three-body interactions using three-body observables, and so on. Another option is to fix all LECs simultaneously to the selection of observables in a range of different nuclei. We could also do something in between, fixing the two-body LECs using two-body observables and the others using a selection of many-body observables.
- *Electroweak operators*: Coupling photons and weak-interaction bosons to the constituents of a chiral EFT formulation gives access to electromagnetic and weak interaction operators that become relevant for the computation of electromagnetic or weak transitions in nuclei. They can be derived consistently in chiral EFT, which is another great advantage of this approach.

All these aspects are active fields of debate and research today. The different options on chiral order, many-body forces, regulator scheme and scale, and strategy for LEC determination lead to a growing collection of nuclear interactions from chiral EFT that are available for nuclear structure calculations [13, 14, 15, 16, 17, 18, 19, 20, 21, 22, 23]. On top of these choices, there are more fundamental questions

regarding, e.g., the specific choice of degrees-of-freedom or the power counting and renormalizability, that require further research on the EFT side [24, 25].

For many-body practitioners and those who compare ab initio results it is important to understand that there is no 'single' or 'best' chiral EFT interaction. There will always be a variety of different realizations that are conceptually equally valid, but might yield different many-body predictions. Even if all other variables are eliminated, chiral EFT interactions will always come at different chiral orders and the convergence of this expansion has to be explored.

3.3 Uncertainty Quantification

The different choices at the chiral EFT level provide an opportunity to systematically quantify uncertainties in the theoretical description of the Hamiltonian and to propagate these uncertainties to the many-body observables [26].

The paradigm that the theory uncertainties resulting from the modelling of the Hamiltonian should be quantified, has entered ab initio nuclear structure theory only recently. The tools and protocols for this uncertainty quantification (UQ) are still in their infancy. Because of the many different design choices and truncations involved in the construction of chiral interactions, there is no complete protocol yet.

The simplest starting point for an UQ protocol is the convergence of an observable obtained with increasing order of the chiral expansion. For the moment we assume that the many-body calculations are precise, i.e., we do not consider additional uncertainties due to the many-body approach. Assuming that an observable $X^{(n)}$ at chiral order n follows the same power-series expansion in the small parameter Q as the interaction, we can try to estimate the remainder of the truncated series based on the behavior of the finite number of terms we have access to. One can use a simple heuristic scheme [27, 28, 29] based the differences $\Delta X^{(n)} = X^{(n)} - X^{(n-1)}$ in the observable in subsequent lower orders, scaled with expansion parameter to estimate the remainder, e.g. through $\delta X^{(n)} = \max\{Q\Delta X^{(n)}, Q^2\Delta X^{(n-1)}, ...\}$. There are more elaborate schemes using Bayesian statistics to model the distribution of the remainders [30, 31, 32], e.g., the pointwise model presented in [33] that is being used routinely.

Applying these schemes is simple. However, in order to assess the chiral truncation uncertainty, e.g., at order N^3LO, we have to compute the observable for all orders up to N^3LO. Therefore, the computational cost for predicting the observable with uncertainties is four times that of computing just the observable. This is a recurring theme—a systematic uncertainty quantification (in contrast to guesswork) increases the total computational cost significantly.

Another starting point for UQ is the propagation of the statistical uncertainties related to the LEC determination into many-body observables. This requires the construction of sets of interactions (at each chiral order) that sample the LECs as to reproduce the fit observables within their experimental uncertainties. This has been explored for N^2LO interactions, e.g., in [34]. Obviously, propagating statistical un-

certainties requires an even larger number of many-body calculations or emulations of such many-body calculations.

4 Preconditioning

Now that we have specified the Hamiltonian, we can start to work on the solution of the Schrödinger equation. The general strategy for this was laid out in Sect. 2. The critical element in all applications of basis-expansion methods is convergence of the observables with model-space size. This eventually limits the range of applicability of specific many-body schemes, because the computational cost grows dramatically with model-space size and eventually defines a largest feasible basis size. If a specific observable for a given nucleus does not reach a sufficient level of convergence within these model-space limits, then an accurate prediction will not be possible. So some obvious questions are: Are there ways to accelerate the convergence of a given basis-expansion approach? Is it possible to pre-condition the eigenvalue problem such that smaller model spaces are sufficient to reach convergence? Can this be done without modifying the physics outputs of such a calculation? Luckily, the answer to all these question is: yes!

The most direct way to pre-condition the many-body problem consists in a transformation of the Hamiltonian itself, and we will discuss this option in Sect. 4.1 and 4.2. Another way to accelerate the convergence in the context of a basis-expansion approach is the choice of an optimized single-particle basis, as explored in Sect. 4.3. Finally, we can simplify the numerical treatment with an approximate inclusion of many-body forces through normal-ordering techniques discussed in Sect. 4.4.

4.1 Unitary Transformations, Prediagonalization and Correlations

The most efficient way to precondition the many-body problem in a basis-expansion approach is a transformation of the Hamiltonian itself with the aim to accelerate the convergence. We want to arrive at converged observables in smaller model spaces, the smaller the better, because this will allow us to tackle heavier nuclei. However, the transformation should not change the results of the many-body calculation—all observables should be invariant under the transformation.

A general class of transformations that formally guarantees the invariance of observables are unitary transformations. Assume a unitary operator $\hat{U}$ with $\hat{U}^{\dagger}\hat{U} = \hat{1} = \hat{U}\hat{U}^{\dagger}$. The unitary transformation of the Hamiltonian is then given by

$$\hat{\bar{H}} = \hat{U}^{\dagger}\hat{H}\hat{U} \ . \tag{11}$$

A key property of unitary transformation is that they do not change the spectrum of the transformed Hamiltonian, i.e., all eigenvalues are invariant. This can be shown

starting from the eigenvalue equation for $\hat{H}$ and by inserting $\hat{U}\hat{U}^\dagger$ and multiplying with $\hat{U}^\dagger$:

$$\hat{H}\,|\Psi_n\rangle = E_n\,|\Psi_n\rangle \;\Leftrightarrow\; \hat{U}^\dagger\hat{H}\hat{U}\hat{U}^\dagger\,|\Psi_n\rangle = E_n\hat{U}^\dagger\,|\Psi_n\rangle \;\Leftrightarrow\; \hat{\tilde{H}}\,|\tilde{\Psi}_n\rangle = E_n\,|\tilde{\Psi}_n\rangle\,,$$
(12)

where we have introduced the transformed eigenstates $|\tilde{\Psi}_n\rangle = \hat{U}^\dagger\,|\Psi_n\rangle$. By solving the eigenvalue problem of $\hat{\tilde{H}}$ we obtain the same energy eigenvalues E_n with the transformed eigenstates. Considering other observables obtained from the energy eigenstates, e.g., through expectation values of an operator $\hat{O}$, we can perform a similar calculation inserting $\hat{U}\hat{U}^\dagger$ twice:

$$O_n = \langle\Psi_n|\,\hat{O}\,|\Psi_n\rangle = \langle\Psi_n|\,\hat{U}\hat{U}^\dagger\hat{O}\hat{U}\hat{U}^\dagger\,|\Psi_n\rangle = \langle\tilde{\Psi}_n|\,\hat{\tilde{O}}\,|\tilde{\Psi}_n\rangle \qquad (13)$$

with the transformed operator

$$\hat{\tilde{O}} = \hat{U}^\dagger\hat{O}\hat{U}\,. \qquad (14)$$

Thus, also expectation values and matrix elements can be computed using the transformed eigenstates $|\tilde{\Psi}_n\rangle$ together with the consistently transformed operator $\hat{\tilde{O}}$.

In summary, many-body observables are invariant under unitary transformations. When solving the many-body problem with the transformed Hamiltonian we only have to make sure that observables are evaluated with consistently transformed operators. Two questions remain: (1) What does the unitary transformation have to do to the Hamiltonian to accelerate model-space convergence? (2) How to formulate and implement such a transformation?

Imagine the matrix representation of the Hamiltonian in a large (infinite) many-body basis, where all regions of the matrix are populated with non-zero matrix elements. If we now truncate the basis to a small (finite) model space, and only solve the eigenvalue problem of the small matrix, the eigenvalues and eigenvectors will change as compared to the full matrix. This could be avoided if the full matrix would have a block-diagonal structure, i.e., if the model space would form one block and the rest of the Hilbert space would form the other block and all the matrix elements connecting the two blocks would be zero. Solving the eigenvalue problem in the small model space would reproduce part of the spectrum of the full matrix.

This block-diagonalization or block-decoupling idea with respect to the actual model space of the many-body calculation, the so-called P-space, and the excluded part of the Hilbert space, the so-called Q-space, is at the heart of the Okubo-Lee-Suzuki (OLS) transformation [35, 36]. In OLS a similarity transformation is constructed explicitly from the formal decoupling condition, i.e., the requirement that the transformed Hamiltonian should not connect P and Q-space. We will not go into the formalism, but just remark that, by construction, the resulting transformed Hamiltonian will depend on nucleus, single-particle basis, and model-space. This results in a non-trivial convergence behavior as function of model-space size, which makes an uncertainty quantification difficult.

It would be advantageous to construct a transformation that performs a pre-diagonalization in a more generic sense, independent of the specific nucleus and

model space, with a transformed interaction that is *universal* and can be employed in any basis expansion approach. Such a method will not provide a perfect block-decoupling of a model space, but it will nonetheless accelerate the convergence and provide a regular convergence behavior that obeys the variational principle.

A first method that implemented generic unitary transformations in this spirit is the unitary correlation operator method (UCOM) [37, 38, 39]. Here we explicitly design the operator for the unitary transformation, guided by the structure of the interaction and the physics of correlations induced in the many-body states. The UCOM concept highlights the intimate connection between decoupling and correlations.

As a reminder, correlations are a property of many-body states that distinguish them from states of a system of non-interacting, independent particles. The eigenstates of a system of non-interacting fermions are Slater-determinants, i.e., the basis states we typically use in our basis expansion approaches. A strongly correlated state can only be represented by a superposition of a huge number of Slater determinants. Looking at the structure of the Hamilton matrix, a Hamiltonian with many strong off-diagonal matrix elements will induce more correlations, because these off-diagonal matrix elements are generating the admixture of the corresponding basis states to the eigenstates. A Hamiltonian with fewer off-diagonal matrix elements will generate less admixtures, weaker correlations, and faster convergence. An extensive discussion of UCOM and the concept of correlations can be found in [39].

Over the past decade a new method has essentially replaced OLS, UCOM, and similar approaches in many applications. The reason for its success is the simplicity and flexibility of the underling formulation. This method is the similarity renormalization group, which will be discussed in detail in the following sections.

4.2 Similarity Renormalization Group

4.2.1 General Idea

The similarity renormalization group (SRG) transformation is the most elegant and versatile way to implement a unitary transformation to pre-diagonalize the Hamiltonian. It goes back to Wegner [40, 41] as well as Glazek and Wilson [42], it was adopted in nuclear structure physics in 2007 [43] and has thrived since then [39, 44, 45, 46].

We start by formulating a continuous unitary transformation of the initial Hamiltonian $\hat{H}$

$$\hat{H}(\alpha) = \hat{U}^{\dagger}(\alpha)\, \hat{H}\, \hat{U}(\alpha)\,, \tag{15}$$

using a unitary transformation operator $\hat{U}(\alpha)$, which depends on a continuous parameter α, the so-called *flow parameter*. The unitarily transformed Hamiltonian $\hat{H}(\alpha)$ now also depends on the flow parameter. For $\alpha = 0$ we define an initial condition requiring that $\hat{U}(\alpha = 0) = \hat{1}$ so that the evolved Hamiltonian coincides with the initial Hamiltonian $\hat{H}(\alpha = 0) = \hat{H}$.

Formally, we can take the derivative of eq. (15) with respect to the flow parameter α, which leads to

$$
\begin{aligned}
\frac{d}{d\alpha}\hat{H}(\alpha) &= \left(\frac{d}{d\alpha}\hat{U}^{\dagger}(\alpha)\right)\hat{H}\,\hat{U}(\alpha) + \hat{U}^{\dagger}(\alpha)\,\hat{H}\left(\frac{d}{d\alpha}\hat{U}(\alpha)\right)\\
&= \left(\frac{d}{d\alpha}\hat{U}^{\dagger}(\alpha)\right)\hat{U}(\alpha)\,\hat{H}(\alpha) + \hat{H}(\alpha)\,\hat{U}^{\dagger}(\alpha)\left(\frac{d}{d\alpha}\hat{U}(\alpha)\right),
\end{aligned}
\tag{16}
$$

where we have inserted the unitarity relation $\hat{U}^{\dagger}(\alpha)\,\hat{U}(\alpha) = \hat{1}$ to recover the transformed Hamiltonian $\hat{H}(\alpha)$. We now define the so-called *generator* $\hat{\eta}(\alpha)$ through

$$
\hat{\eta}(\alpha) = -\hat{U}^{\dagger}(\alpha)\left(\frac{d}{d\alpha}\hat{U}(\alpha)\right).
\tag{17}
$$

From the flow-parameter derivative of the unitarity relation $\hat{1} = \hat{U}^{\dagger}(\alpha)\,\hat{U}(\alpha)$ we find that the generator is an anti-hermitean operator, i.e., $\hat{\eta}^{\dagger}(\alpha) = -\hat{\eta}(\alpha)$. Combining all this leads to the final form of the SRG *flow equation*

$$
\frac{d}{d\alpha}\hat{H}(\alpha) = [\hat{\eta}(\alpha), \hat{H}(\alpha)].
\tag{18}
$$

The steps from eq. (15) to this flow equation are very general and do not rely on any specifics of the transformation. The difference between the flow equation (18) and the direct transformation (15) lies in inputs needed to evaluate the transformed Hamiltonian: For the direct transformation we have to specify the unitary operator $\hat{U}(\alpha)$, for the flow equation we only need to define the generator $\hat{\eta}(\alpha)$.

There are many different ways to define the generator $\hat{\eta}(\alpha)$. The simplest and most intuitive choice goes back to Wegner [40, 41] and is based on the commutator of the transformed Hamiltonian $\hat{H}(\alpha)$ with its 'diagonal part' $\hat{H}^{d}(\alpha)$

$$
\hat{\eta}_{\mathrm{W}}(\alpha) = [\hat{H}^{d}(\alpha), \hat{H}(\alpha)] = [\hat{H}^{d}(\alpha), \hat{H}^{od}(\alpha)].
\tag{19}
$$

Identifying the diagonal and off-diagonal parts of the Hamiltonian requires a matrix representation of the Hamiltonian with respect to some specific basis. One can identify the diagonal part with the strict diagonal of the Hamilton matrix, or one can use more general band or block-diagonal structures to identify $\hat{H}^{d}(\alpha)$. The off-diagonal part then follows via $\hat{H}^{od}(\alpha) = \hat{H}(\alpha) - \hat{H}^{d}(\alpha)$.

Irrespective of the specific choice, the flow equation will suppress the off-diagonal part of the Hamiltonian throughout the flow evolution. If the Hamiltonian has reached a perfect diagonal form, then $\hat{H}^{od}(\alpha) = 0$, the generator (19) vanishes, and the flow evolution stops—this defines the fix point of the SRG flow evolution.

This is the most important aspect of the SRG, it provides a simple and elegant way to pre-diagonalize the Hamiltonian with respect to a specific basis. The choice of the generator defines which basis this is and how exactly the pattern of diagonal and off-diagonal pieces should look like. This makes the whole approach very flexible and intuitive. It turns out that it is much simpler to construct a generator that drives a

specific, physics-motivated pre-diagonalization than to formulate the corresponding unitary operator directly.

As indicated earlier, instead of thinking in terms of diagonalization one can also think in terms of *decoupling*. Any suppression of off-diagonal matrix elements entails a decoupling of certain parts of the basis from the rest of the basis. For a generator that drives the Hamiltonian towards a block-diagonal structure, the individual blocks would eventually decouple and it would suffice to solve the eigenvalue problem for an individual block to recover a part of the exact spectrum.

4.2.2 Consistent Observables

When using a unitarily transformed Hamiltonian (15) in a subsequent many-body calculation, we have to make sure that the operators of all other observables of interest are transformed consistently (cf. Sect. 4.1). Thus, for a generic observable $\hat{O}$ we have to evaluate the transformation

$$\hat{O}(\alpha) = \hat{U}^{\dagger}(\alpha)\,\hat{O}\,\hat{U}(\alpha)\,. \tag{20}$$

We can use the same steps as for the Hamiltonian to convert this explicit unitary transformation into flow equation

$$\frac{d}{d\alpha}\hat{O}(\alpha) = [\hat{\eta}(\alpha), \hat{O}(\alpha)]\,, \tag{21}$$

with the initial condition $\hat{O}(\alpha = 0) = \hat{O}$. Note that the antihermitean generator $\hat{\eta}(\alpha)$ has to be the same as in the flow equation of the Hamiltonian. Since the generator necessarily contains the evolved Hamiltonian, we have to solve the flow equation for $\hat{H}(\alpha)$ as well. To handle this numerically, the two flow equations (18) and (21) are solved simultaneously as a coupled system of differential equations of twice the size. If there is only one other observable of interest, then this is usually no problem, however, it is getting tedious if several operators have to be transformed.

A more elegant way is the construction of the unitary transformation $\hat{U}(\alpha)$ itself. We can recast equation (17), by multiplying from the left with the unitary operator $\hat{U}(\alpha)$, into a differential equation for $\hat{U}(\alpha)$

$$\frac{d}{d\alpha}\hat{U}(\alpha) = -\hat{U}(\alpha)\,\hat{\eta}(\alpha)\,. \tag{22}$$

This differential equation again involves the generator which depends on the evolved Hamiltonian and, therefore, has to be solved simultaneously with the flow equation (18). However, once this is done we have a representation of the unitary operator $\hat{U}(\alpha)$ which can be used to explicitly transform any other operator (including the Hamiltonian) using (20).

In a numerical setting where (22) is integrated stepwise starting from the initial condition $\hat{U}(\alpha = 0) = \hat{1}$, there is also the option to compute the Hamiltonian $\hat{H}(\alpha)$ entering the generator from an explicit transformation (15) with the $\hat{U}(\alpha)$ obtained

in the previous integration step. In this way we only need to handle one differential equation.

There is a third way to handle the general transformation of operators, the so-called Magnus expansion [47, 48]. It is similar to the solution of the differential equation for $\hat{U}(\alpha)$, but this time we first parametrize the unitary operator $\hat{U}(\alpha)$ in terms of an anti-hermitean Magnus operator $\hat{\Omega}(\alpha)$ through

$$\hat{U}(\alpha) = \exp(-\hat{\Omega}(\alpha)) \tag{23}$$

with $\hat{\Omega}(\alpha = 0) = 0$. One might be tempted to think that the Magnus operator is the same as the generator $\hat{\eta}(\alpha)$—it is not. Since the generator $\hat{\eta}(\alpha)$ depends on α itself and does not commute with itself for different values of the flow parameter, the formal integration of (22) does not simply yield an exponential of the generator. This is exactly what the Magnus expansion takes care of.

The Magnus operator can be obtained from the following differential equation

$$\frac{d}{d\alpha}\hat{\Omega}(\alpha) = \sum_{k=0}^{\infty} \frac{B_k}{k!} [\hat{\Omega}(\alpha), \hat{\eta}(\alpha)]_k \ , \tag{24}$$

where B_k are the Bernoulli numbers and $[\hat{X}, \hat{Y}]_k = [\hat{X}, [\hat{X}, ...[\hat{X}, \hat{Y}]]]$ are the k-fold nested commutators, where k gives the number of $\hat{X}$ factors, i.e., $[\hat{X}, \hat{Y}]_0 = \hat{Y}$, $[\hat{X}, \hat{Y}]_1 = [\hat{X}, \hat{Y}]$, etc. We will not be able to handle the infinite series on the right-hand-side exactly, we have to truncate this series in finite order. The good news is that no matter how bad this truncation for $\hat{\Omega}(\alpha)$ is, it will not destroy the unitarity of the transformation. Another technical benefit is that for typical applications, the differential equation (24) is numerically easier to handle (less stiff) and thus more efficient to solve (fewer and larger steps).

Once we have obtained $\hat{\Omega}(\alpha)$, we still have to evaluate the unitary transformation of the observables through (20) and (23). This can be done via another expansion, the Baker-Campbell-Hausdorff series

$$\hat{O}(\alpha) = \exp(+\hat{\Omega}(\alpha)) \ \hat{O} \ \exp(-\hat{\Omega}(\alpha)) = \sum_{n=0}^{\infty} \frac{1}{n!} [\hat{\Omega}(\alpha), \hat{O}]_n \tag{25}$$

using nested commutators. Again, we will have to truncate this infinite series in numerical applications, but typically this series converges rather quickly. Note that this truncation might destroy the unitarity of the transformation.

It might seem that the Magnus approach only causes complications and, indeed, whenever a direct construction of $\hat{U}(\alpha)$ through (22) is possible this will be the preferred method. However, the Magnus expansion will have important applications in an advanced version of SRG that will be discussed in Sect. 6.1.

4.2.3 Free-Space Similarity Renormalization Group

So far, we have discussed a generic version of the SRG at the operator level. The Hamiltonian in this discussion is the Hamiltonian for the A-body system and the basis used to identify diagonal and off-diagonal parts is the full A-body basis, as introduced in Sect. 2, or at least an A-body basis in a huge model space. Therefore, we have gained nothing regarding to the computational complexity of the problem— it is more challenging to solve a coupled system of differential equations for the matrix elements in a huge model space than to solve the eigenvalue problem of this matrix. We have to use the SRG evolution in a different setting to really gain something. There are two such beneficial settings that we will discuss in this lecture, the free-space SRG and the in-medium SRG.

The free-space SRG is build on two design choices: (i) The use of a generator that yields a basis-independent transformation and implements a more generic decoupling idea; (ii) The evaluation of the SRG flow equations in few-body spaces, typically $A = 2$ and $A = 3$ and a subsequent embedding of the evolved operators into A-body space via a cluster expansion.

Let us first discuss the generator that is most widely used in the free-space SRG. To construct a universal Hamiltonian for use in a wide array of many-body methods for different nuclei, we adopt a more generic concept of pre-diagonalization or decoupling—and the concept that comes to mind is the decoupling of energy or momentum scales. We could use the diagonal of the Hamiltonian in the eigenbasis of the total momentum or the kinetic energy operator. Or even simpler, we can use the kinetic energy operator directly, instead of the diagonal part of the Hamiltonian. This leads to the SRG generator that was introduced in [49, 43] and is widely used in nuclear physics

$$\hat{\eta}_T(\alpha) = \frac{m^2}{\hbar^4} \, [\hat{T}_{\text{int}}, \hat{H}(\alpha)] \,, \tag{26}$$

where $\hat{T}_{\text{int}}$ is the intrinsic kinetic energy (9) and the prefactor including the nucleon mass m is chosen such that the flow-parameter α has units [length^4]. For this specific generator it is reasonable to associate the flow parameter with a momentum scale λ, using the relation $\lambda = \alpha^{-1/4}$.

Using this generator, the SRG flow equations will drive the Hamiltonian towards a band-diagonal form in momentum representation. In other words, it decouples low-momentum states from high-momentum states, since the matrix elements far-off the diagonal in a momentum representation are suppressed. This suppression will also be effective in other basis representations, e.g. the harmonic-oscillator basis, we will illustrate this in Sect. 4.2.5.

4.2.4 Cluster Expansion & Cluster Truncation

Despite the simplicity of the equations, we cannot evaluate the flow equations at the general A-body level. However, we can evaluate them in few-body systems, typically

$A = 2$ and $A = 3$, and reconstruct the evolved operator in A-body space from this in an approximate way. The formal background of this procedure is the so-called *cluster expansion* and a *cluster truncation*.

We can decompose the transformed Hamiltonian $\hat{H}(\alpha)$ for the A-body system into irreducible k-body operators $\hat{H}^{[k]}$

$$\hat{H}(\alpha) = \hat{H}^{[1]}(\alpha) + \hat{H}^{[2]}(\alpha) + \hat{H}^{[3]}(\alpha) + \cdots + \hat{H}^{[A]}(\alpha) \ . \tag{27}$$

Each k-body operator of the cluster expansion can be written in its second-quantized form with k-body matrix elements $H_{q_1...q_k}^{p_1...p_k}(\alpha) = \langle p_1...p_k| \hat{H}^{[k]}(\alpha) |q_1...q_k\rangle$ and a product of k creation and k annihilation operators

$$\hat{H}^{[k]}(\alpha) = \frac{1}{(k!)^2} \sum_{p_1,...,p_k} \sum_{q_1,...,q_k} H_{q_1...q_k}^{p_1...p_k}(\alpha) \, \hat{a}_{p_1}^{\dagger} \cdots \hat{a}_{p_k}^{\dagger} \hat{a}_{q_k} \cdots \hat{a}_{q_1} \tag{28}$$

To work out the individual terms of the cluster expansion, i.e., the matrix elements $H_{q_1...q_k}^{p_1...p_k}(\alpha)$ for $k = 1, 2, 3, ...$, we simply perform the SRG transformation of the Hamiltonian in Hilbert spaces of increasing particle number A. For $A = 1$ the SRG transformation does not do anything, since the generator does not have a one-body contribution, so the one-body part of the transformed Hamiltonian equals the initial one-body part. For $A = 2$ we get a non-trivial transformation of the Hamiltonian. After subtraction of the previously obtained one-body part embedded into two-body space, this yields the irreducible two-body part. For $A = 3$ we again get a transformed Hamiltonian that, after subtraction of the previously determined one and two-body contributions, yields the irreducible three-body part [39, 45, 50].

This scheme continues up to the A-body level. Even if the initial Hamiltonian only has up to three-body terms, because we only include up to 3N interactions, the transformed Hamiltonian contains induced terms beyond the three-body level. These induced multi-particle contributions formally have to be included to warrant the unitarity of the transformation and to benefit from exact unitary equivalence discussed in Sect. 4.1. Induced multi-particle interactions are the price to pay for the improved convergence with the transformed Hamiltonian—a clear case of the no-free-lunch theorem.

For the SRG transformation it is easy to see, how induced multi-particle terms emerge. Consider the SRG-flow equation (18) with the free-space SRG generator (26). Now we solve the flow-equation as an initial value problem in a simplistic Euler-type approach, i.e., we assume a small step $\Delta\alpha$ in the flow-parameter and use a two-point finite difference form to approximate the derivative of the Hamiltonian. After simple rearrangements we get for one Euler step

$$\hat{H}(\alpha + \Delta\alpha) \approx \hat{H}(\alpha) + \Delta\alpha \frac{m^2}{\hbar^4} [[\hat{T}_{\text{int}}, \hat{H}(\alpha)], \hat{H}(\alpha)] \ . \tag{29}$$

For simplicity we assume that the initial Hamiltonian $\hat{H}(\alpha = 0)$ only consists of a two-body term and we recall that the intrinsic kinetic $\hat{T}_{\text{int}}$ can also be written as a two-body operator. We can now use a general property of commutators: The commutator

of an n-body and an m-body operator yields contributions up to $(n + m - 1)$-body operators. Thus, the commutator of two two-body operators produces up to three-body operators, and the nested-commutator of three two-body operator generates up to four-body operators. As a consequence, a single Euler step from $\alpha = 0$ to $\alpha = \Delta\alpha$ induces up to four-body terms in the Hamiltonian. And the many small Euler steps needed to reach a finite flow parameter will induce multi-particle terms of arbitrary particle rank.

Obviously, we cannot keep all induced multi-particle interactions in practical calculations. First of all, it is computationally not possible to solve the SRG flow equations for larger A—we can routinely handle the evolution in three-body space, but already the evolution in four-body space is not fully tractable at present. Second, even if the all induced multi-particle terms would be available, their inclusion in the final many-body calculation would be prohibitive. Already the step from two-body to three-body interactions significantly increases the computational complexity, and some approaches are still not able to include three-body interactions without additional approximation.

Therefore, we have to truncate the cluster expansion at finite particle-numbers and by this introduce an approximation at the level of the Hamiltonian. Remember that already the initial Hamiltonian constructed within chiral EFT is subject to truncations with respect to chiral order and multi-particle interactions, and the truncation of the cluster expansion can be viewed in the same context. The present state-of-the-art is to include the chiral interactions up to the three-body level and to truncate the evolved Hamiltonian also at the three-body level [50, 51, 45].

In this situation it is important to quantify the uncertainties resulting from the cluster truncation. Luckily, the SRG offers a handy tool to assess these truncation uncertainties without explicitly calculating the next order of the expansion. We can use the continuous flow parameter α as a diagnostic. Because the un-truncated SRG evolution is unitary and preserves the spectrum and the observables, any dependence of the energy eigenvalues or other observables on the flow parameter in a converged many-body calculation using truncated operators signals the impact of discarded multi-particle terms in the cluster expansion [50, 51, 45].

4.2.5 Example: SRG Evolution in Three-Body Space

As an illustration of the free-space SRG transformation we consider the three-body system, corresponding illustrations for the simpler two-body system can be found in the literature [44, 39].

In order to numerically solve the SRG flow equation for the Hamiltonian in three-body space, we need an appropriate basis to convert the operator flow-equation (18) into a set of coupled differential equations for the matrix elements. We will use a harmonic oscillator basis in the relative coordinates of the three-particle system, the so-called Jacobi coordinates. The antisymmetrized states of the relative harmonic-oscillator basis, which will be discussed in more detail in Sect. 4.3.1, can be written as $|E i J^\pi M, T M_T\rangle$, with a three-particle principal quantum number E and a collective
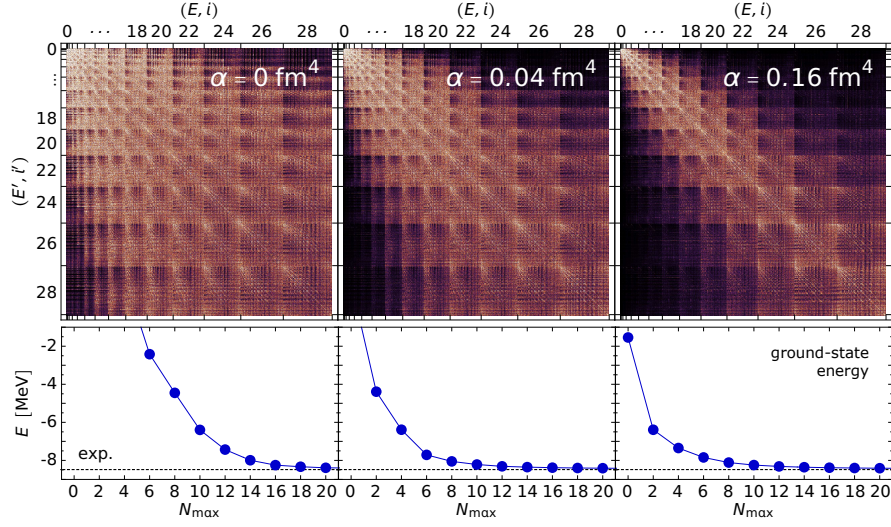
Fig. 1 Three-body matrix elements (top panels) and ground-state energy convergence (bottom panels) for the triton with initial and SRG-evolved NN+3N interactions. Modified from [50].

quantum number i that encapsulates the orbital angular momentum and spin degrees of freedom [50].

The matrix elements of the initial chiral NN+3N interaction in this basis for the quantum numbers of the triton, i.e., $J^{\pi} = 1/2^+$, $T = 1/2$, $M_T = -1/2$, are depicted in the top-left panel of Fig. 1. The rows and columns are spanned by the quantum numbers (E, i), where the apparent block-structure results from sections of the basis with fixed E. The lower-left panel shows the lowest eigenvalues resulting for the numerical solution of the eigenvalue problem of the corresponding Hamilton matrix, truncated to $E \leq N_{\max}$—as will be discussed later, this corresponds to a Jacobi no-core shell model calculation for the triton ground state. We observe that the matrix has strong off-diagonal matrix elements and that the ground-state energy needs large model spaces with $N_{\max} \gtrsim 16$ to converge. The next two columns show the matrix elements and energies for the SRG evolved interaction for flow parameter $\alpha = 0.04 \, \text{fm}^4$ and $0.16 \, \text{fm}^4$, respectively. The matrices clearly show the suppression of off-diagonal matrix elements with increasing flow parameter—note that although we use the kinetic energy generator (26) here, the pre-diagonalization is also evident in an harmonic-oscillator basis. The corresponding plots for the ground-state energies show a much faster convergence, now $N_{\max} \approx 8$ is sufficient to reach the same level of convergence as reached at $N_{\max} \approx 16$ for the initial interaction. The converged energy is the same in all cases, since the SRG transformation includes all three-body terms.

4.3 Single-Particle Basis

The convergence behavior of basis expansion calculations also depends on the choice of the underlying single-particle basis. We can try to optimize this basis with respect to global properties of the nucleus, e.g., its spatial size. Obviously, the convergence will deteriorate if we choose basis sets spanning length scales that are completely different from the intrinsic length scale of the nucleus. We will discuss three types of single-particle bases for the description of finite nuclei: the harmonic-oscillator basis, the Hartree-Fock basis, and a specific variant of a natural-orbital basis.

4.3.1 Harmonic Oscillator Basis

The harmonic oscillator (HO) is the default basis for any type of localized many-body system, simply because the basis functions are analytically known and there are many special relations for the HO basis that are of critical importance for practical calculations.

When we talk about the HO basis, we refer to the eigenstates of a single particle in a spherical harmonic-oscillator potential characterized by an oscillator frequency Ω or an oscillator length $a = \sqrt{\hbar/(m\Omega)}$. The single-particle HO Hamiltonian reads

$$\hat{h}_{\text{HO}} = \frac{1}{2m}\,\hat{\mathbf{p}}^2 + \frac{m\Omega^2}{2}\,\hat{\mathbf{x}}^2 \ . \tag{30}$$

The analytic solution of the eigenvalue problem of this Hamiltonian can be found in any textbook on quantum mechanics. We exploit spherical symmetry and introduce orbital angular momentum quantum numbers l and m_l plus an addition radial quantum number n, so that the eigenstates are characterized as $|nlm_l\rangle$. The energy eigenvalues are given by $\epsilon_{nl} = \hbar\Omega(2n + l + 3/2) = \hbar\Omega(e + 3/2)$ with the principal quantum number $e = 2n + l$. The spectrum is equidistant with a fixed energy spacing $\hbar\Omega$ between adjacent single-particle levels.

There is one feature that makes the HO unique and directly results from the fact the the HO Hamiltonian is a quadratic form in position and momentum. If we consider two classical particles of mass m with positions $\mathbf{x}_1$ and $\mathbf{x}_2$, then we can introduce a relative coordinate $\mathbf{r} = \mathbf{x}_1 - \mathbf{x}_2$ and a center-of-mass coordinate $\mathbf{X} = \frac{1}{2}(\mathbf{x}_1 + \mathbf{x}_2)$. We can extend this to the momenta of the two particles $\mathbf{p}_1$ and $\mathbf{p}_2$ and define a relative momentum $\mathbf{q} = \frac{1}{2}(\mathbf{p}_1 - \mathbf{p}_2)$ and a total or center-of-mass momentum $\mathbf{P} = \mathbf{p}_1 + \mathbf{p}_2$. We can do the same with the position and momentum operators in quantum mechanics and, because of our choice of prefactors, the canonical commutation relations between position and momentum operators also hold for the relative and center-of-mass operators.

We can transfer this to the (classical or quantum) Hamiltonian of a system of two non-interacting particles in a HO potential and write it either using the single-particle operators or the relative and center-of-mass operators. A simple calculation shows that

$$\hat{h}_{\text{HO},1} + \hat{h}_{\text{HO},2} = \frac{1}{2m}\, \hat{\mathbf{p}}_1^2 + \frac{m\Omega^2}{2}\, \hat{\mathbf{x}}_1^2 + \frac{1}{2m}\, \hat{\mathbf{p}}_2^2 + \frac{m\Omega^2}{2}\, \hat{\mathbf{x}}_2^2$$

$$= \frac{1}{2\mu}\, \hat{\mathbf{q}}^2 + \frac{\mu\Omega^2}{2}\, \hat{\mathbf{r}}^2 + \frac{1}{2M}\, \hat{\mathbf{P}}^2 + \frac{M\Omega^2}{2}\, \hat{\mathbf{X}}^2 = \hat{h}_{\text{HO,rel}} + \hat{h}_{\text{HO,cm}}$$

(31)

with the reduced mass $\mu = m/2$ and the total mass $M = 2m$. In the second line we have identified a HO Hamiltonian $\hat{h}_{\text{HO,rel}}$ in the relative quantities and a HO Hamiltonian $\hat{h}_{\text{HO,cm}}$ for the center-of-mass quantities. The first line tells us, that a tensor product of two single-particle HO states, i.e., $|n_1 l_1 m_{l1}\rangle \otimes |n_2 l_2 m_{l2}\rangle$, will be an eigenstate of this two-body Hamiltonian with an energy eigenvalue $\hbar\Omega(e_1 + e_2 + 3)$. The second line tells us that a tensor product of HO eigenstates for the relative motion $|n_{\text{rel}} l_{\text{rel}} m_{l,\text{rel}}\rangle$ and the center-of-mass motion $|n_{\text{cm}} l_{\text{cm}} m_{l,\text{cm}}\rangle$ is also an eigenstate with eigenvalue $\hbar\Omega(e_{\text{rel}} + e_{\text{cm}} + 3)$. Thus we have two different eigenbasis sets for the same Hamiltonian, spanning the same two-particle Hilbert space with the same degenerate sub-spaces for the two-body principal quantum number $E_2 = e_1 + e_2 = e_{\text{rel}} + e_{\text{cm}}$. Therefore, there has to be a unitary transformation connecting the states of the two bases within each of the degenerate subspaces. This basis transformation is the celebrated Talmi or Talmi-Moshinsky-Smirnov transformation [52, 53, 54]

$$|n_{\text{rel}} n_{\text{cm}}[l_{\text{rel}} l_{\text{cm}}]LM_L\rangle = \sum_{n_1, n_2, l_1, l_2} \langle\!\langle n_1 n_2, l_1 l_2; n_{\text{rel}} n_{\text{cm}}, l_{\text{rel}} l_{\text{cm}}; L \rangle\!\rangle\ |n_1 n_2[l_1 l_2]LM_L\rangle\,,$$

(32)

where the sum is restricted to $e_{\text{rel}} + e_{\text{cm}} = e_1 + e_2$. For convenience we have coupled the two orbital angular momenta in each basis to total orbital angular momentum L and M_L. The transformation coefficients $\langle\!\langle n_1 n_2, l_1 l_2; n_{\text{rel}} n_{\text{cm}}, l_{\text{rel}} l_{\text{cm}}; L \rangle\!\rangle$ are the so-called Moshinsky coefficients or harmonic-oscillator brackets [55].

Why is this important? Well, we use this transformation all the time in practical calculations, here are a few examples:

- *Computation of NN matrix elements*: For the many-body calculation we need two-body matrix elements with respect to antisymmetrized product states, as they appear, e.g., in the second-quantized form of a two-body operator. For the computation of the matrix elements of the chiral NN interaction or for the SRG evolution, a relative two-body basis is much more convenient. We can exploit spherical symmetry and the center-of-mass part of the basis separates, which drastically reduces the number of matrix elements. Therefore, we first compute all the relative-HO matrix elements, perform the SRG-transformation in the relative-HO basis, and in the end use the Talmi transformation to compute the matrix elements in terms of single-particle quantum numbers for use in the subsequent many-body calculation.
- *Computation of 3N matrix elements*: This is essentially the same story as for the NN interaction, only more complicated since we have to work with three particles. We need an extension of the relative and center-of-mass coordinates for the three-body system, which leads to the so-called Jacobi-coordinates. This construction of the Jacobi coordinates translates into a corresponding hierarchical nesting of

relative HO quantum numbers and the corresponding Talmi transformations. We refer the reader to [50] for a detailed discussion.

- *Center-of-mass separation*: We can formally extend the idea of the Jacobi coordinates and the corresponding relative HO states and associated Talmi transformation to the many-body level. For an A-body model space spanned by all Slater determinants of HO single-particle states up to a maximum total quantum number $\sum_i e_i \leq E_{A,\max}$, there is an alternative basis of relative and center-of-mass HO states, connected through an A-body Talmi transformation. The relative HO basis allows for an explicit separation of the center-of-mass state of the A-body system from the intrinsic state. Therefore, also the Slater determinant basis in an $E_{A,\max}$-truncated space allows for an exact center-of-mass separation. We will come back to this point in Sect. 5.3.

All of this is unique to the HO and, therefore, we will always use the HO basis at certain stages of the calculation. However, there is also a dark side, related to the asymptotic behavior of the HO wave functions. The potential term in the HO Hamiltonian grows quadratically with $x = |\mathbf{x}|$ and, as a result, the HO coordinate-space wave functions fall off with a Gaussian $e^{-x^2/(2a^2)}$ behavior. This is unrealistic for a self-bound system. If a localized many-particle system is bound by finite-range attractive interaction between the particles, then we can invoke a schematic mean-field-type picture. The average interaction of a particle with all the others will resemble a potential well, which goes to zero in the exterior. The bound single-particle wave functions for such a mean-field potential will fall off exponentially and not like a Gaussian. If we use the HO basis for a many-body calculation, then we have to correct for the unrealistic asymptotic behavior by superpositions of many basis states in order to build up the exponential asymptotic. This will slow down the model-space convergence, particularly for weakly bound states and halo nuclei, which show a prominent exponential tail in their density distribution.

4.3.2 Hartree-Fock Basis

An obvious candidate for a more suitable set of single-particle states is the Hartree-Fock (HF) basis. The HF approximation itself is covered in many textbooks [56, 57], so we keep this discussion brief.

The HF method provides a variational approximation for the ground state of the A-body system assuming a trial state that consists of a single Slater determinant. The variational degrees of freedom are the single-particle states that enter into the trial state. The HF equations that determine the single-particle basis simply result as Euler-Lagrange equations from the minimization of the expectation value of the many-body Hamiltonian with the Slater determinant trial state. This simple picture holds for closed-shell nuclei, where all magnetic sub-states of the highest j-shell are occupied. For the purpose of constructing a basis in open-shell nuclei, we can use a simple constrained HF scheme with an equal-filling approximation for the partially occupied shell.

The HF single-particle basis definitely has advantages. It is constructed from a variational calculation for the nucleus and the Hamiltonian under consideration, using a single Slater determinant that will automatically be a basis state in the subsequent many-body calculation. We can view the subsequent calculation as an expansion around this variational optimum. Global properties of the ground-state that are accessible already in the simplified mean-field picture are build into the many-body basis.

However, it also has some problems. Strictly speaking, the variational approach only constrains the energetically lowest single-particle states that are occupied in the HF ground state. Higher-lying single-particle states are only determined through technical constraints on the density matrix and orthogonality. Furthermore, the HF potential really resembles a potential well with a finite number of bound states with negative single-particle energies. In addition there is a continuous spectrum of solutions at positive energies, representing unbound single-particle states. These unoccupied and unbound states depend on the specific way in which we solve the HF equations. Since our Hamiltonian is specified in term of HO matrix elements, we will represent the HF single-particle states in an HO basis expansion with a truncation with respect to the principal HO quantum number e requiring $e \leq e_{max}$ [58]. The underlying HO basis depends on the oscillator frequency Ω and this dependence carries over particularly to the unoccupied and unbound single-particle states.

Another limitation of the HF basis-optimization is the fact that it does not account for correlations in the many-body state. The HF ground state is a single Slater determinant without any correlations and it is typically far above the exact ground-state energy. Even for SRG-evolved Hamiltonians, HF typically recovers only half of the binding energy. For a bare chiral Hamiltonian, the ground state might not even be bound at the HF level. This mismatch influences the structure of the single-particle states, they are optimized for a badly approximated ground state.

4.3.3 Natural-Orbital Basis

There is a way to inform the single-particle basis about the correlated ground-state of the system and this way involves so-called *natural orbitals*. In general, natural orbitals are single-particle states that result as eigenstates of the one-body density matrix.

We can start from a highly correlated many-body state $|\Psi\rangle$ and compute the one-body density matrix with respect to a specific single-particle basis, e.g. the HO basis, via

$$\rho_{pq} = \langle \Psi | \, \hat{a}_p^\dagger \hat{a}_q \, | \Psi \rangle \, , \tag{33}$$

where the creation and annihilation operators of second quantization are defined with respect to the HO single-particle basis (or any other computational reference basis). We can now solve the matrix-eigenvalue problem of the one-body density matrix, which yields eigenvectors that define the natural-orbital single-particle basis and the eigenvalues the mean occupation numbers of the natural-orbital states.

The natural-orbitals inherit the angular momentum, spin and isospin structure of the reference basis and only differ in the radial wave functions, because a scalar one-body density matrix exhibits a corresponding block structure. So just like in the spherical or constrained HF case, the new single-particle basis can be expressed via a simple basis transformation with respect to the radial quantum numbers

$$|\nu(l\tfrac{1}{2})jm; \tfrac{1}{2}m_t\rangle = \sum_n C_{n\nu}^{(ljm_t)} |n(l\tfrac{1}{2})jm; \tfrac{1}{2}m_t\rangle , \qquad (34)$$

where ν indicates the natural-orbital basis and n the initial HO basis, and the expansion coefficients $C_{n\nu}^{(ljm_t)}$ are given by the eigenvectors of the density matrix.

The interesting question is, how to construct the correlated many-body state $|\Psi\rangle$ that determines the density matrix? Typically, we will consider an approximation for the ground state of the system for the construction of the natural orbitals, although one could also use a density matrix defined for a mixture of states. In principle one can perform a preparatory ab initio calculation, e.g. in a configuration interaction framework, to extract a proxy for the ground state. This has be done [59], but is computationally very expensive.

A much simpler way to construct an approximation for the correlated ground state is many-body perturbation theory [60]. We can start from a HF calculation and add low-order perturbative corrections on top of the unperturbed HF ground state

$$|\Psi\rangle = |\Psi^{(0)}\rangle + |\Psi^{(1)}\rangle + |\Psi^{(2)}\rangle + \ldots \quad \text{with} \quad |\Psi^{(0)}\rangle = |\text{HF}\rangle . \qquad (35)$$

The perturbative corrections $|\Psi^{(i)}\rangle$ $(i > 0)$ account for the most important beyond-HF correlations. Inserting this into the definition of the density-matrix and keeping terms up to the second order in the perturbation yields

$$\rho \approx \rho^{(00)} + \rho^{(02)} + \rho^{(20)} + \rho^{(11)} , \qquad (36)$$

where $\rho^{(00)}$ denotes the unperturbed HF density matrix and

$$\rho_{pq}^{(02)} = \rho_{qp}^{(20)} = \langle\Psi^{(0)}| \hat{a}_p^\dagger \hat{a}_q |\Psi^{(2)}\rangle , \quad \rho_{pq}^{(11)} = \langle\Psi^{(1)}| \hat{a}_p^\dagger \hat{a}_q |\Psi^{(1)}\rangle . \qquad (37)$$

Explicit expressions for these density matrix elements can be found in [60]. With small computational effort, large single-particle spaces can be used to evaluate the perturbative corrections, much larger than the model spaces of the subsequent many-body solution. Thus, the basis can be informed about correlation effects in a very large model space and effectively supply this information for the many-body treatment in a smaller space.

We will use the natural-orbital basis in connection with different many-body approaches and compare the performance of the different basis sets in Sect. 5.3.

4.4 Normal Ordering of Many-Body Interactions

A less obvious preconditioning consists of a rearrangement of the Hamiltonian, the so-called normal ordering. For some of the many-body methods discussed later, normal-ordering is a necessary step to formulate the basic working equations of the method in an efficient way. On top of this, normal ordering can be used to define an approximation for the inclusion of many-body interactions, which presents a major simplification for all many-body methods.

Normal ordering is the simple process for rearranging the order of creation and annihilation operators in the second-quantized form of the Hamiltonian (or any other operator). Let us start with a generic Hamiltonian for the many-body system containing up to three-body operators

$$\hat{H} = \hat{H}^{[1]} + \hat{H}^{[2]} + \hat{H}^{[3]} \ . \tag{38}$$

As in Sect. 4.2.4, $\hat{H}^{[k]}$ represents the k-body part of the Hamiltonian. In second quantization it can be written as

$$\hat{H}^{[k]} = \frac{1}{(k!)^2} \sum_{p_1,\ldots,p_k} \sum_{q_1,\ldots,q_k} H^{p_1\ldots p_k}_{q_1\ldots q_k} \ \hat{a}^\dagger_{p_1} \cdots \hat{a}^\dagger_{p_k} \ \hat{a}_{q_k} \cdots \hat{a}_{q_1} \tag{39}$$

with the shorthand notation $H^{p_1\ldots p_k}_{q_1\ldots q_k} = \langle p_1\ldots p_k | \hat{H}^{[k]} | q_1\ldots q_k \rangle$ for the matrix elements of the k-body part. This is the standard form of an operator in second quantization with the creation operators to the left of the annihilation operators. For later reference, we call this the *vacuum normal-ordered form* of the Hamiltonian. Here, vacuum refers to the vacuum state $|0\rangle$, the only state in the zero-particle Hilbert space, and from the basics of second quantization we remember that $\hat{a}_q |0\rangle = 0$ for all q and thus $\langle 0| \hat{a}^\dagger_p \cdots \hat{a}_q |0\rangle = 0$ and also $\langle 0| \hat{H}^{[k]} |0\rangle = 0$.

Now we start to reinterpret and reshuffle things. Assume a Slater determinant $|\Phi\rangle$, which represents a simplistic approximation for the ground state of a closed-shell system, as obtained, e.g., in a HF calculation. We call this specific Slater determinant the *reference state*. Acting with the annihilation operator $\hat{a}_q$ on the reference state $|\Phi\rangle$ can lead to different results, depending on whether the single-particle state $|q\rangle$ is occupied or unoccupied in the reference state. Using an index convention to distinguish states i, j that are occupied in $|\Phi\rangle$, the *hole states*, from states a, b that are unoccupied in $|\Phi\rangle$, the *particle states*, we find

$$\hat{a}_i |\Phi\rangle \neq 0 \ , \qquad \hat{a}_a |\Phi\rangle = 0 \ , \qquad \hat{a}^\dagger_i |\Phi\rangle = 0 \ , \qquad \hat{a}_a |\Phi\rangle \neq 0 \ . \tag{40}$$

Comparing this to the behavior of annihilation and creation operator applied to the vacuum state $|0\rangle$, we observe that $\hat{a}_a$ and $\hat{a}^\dagger_i$ seem to behave like annihilation operators with respect to $|\Phi\rangle$. Turning this around: $|\Phi\rangle$ behaves like a vacuum state with respect to the set $\hat{a}_a$ and $\hat{a}^\dagger_i$ of annihilation operators. So let us take eq. (39) and rearrange the product of creation and annihilation operators such that at these reinterpreted annihilation operators $\hat{a}_a$ and $\hat{a}^\dagger_i$ are to the right of the reinterpreted

creation operators $\hat{a}_a^\dagger$ and $\hat{a}_i$. This defines normal ordering with respect to the reference state.

Let us convert this into notation. We start from the Hamiltonian $\hat{H}$ and rewrite it in terms of the normal-ordered Hamiltonian $\hat{H}_N$

$$\hat{H} = \langle\Phi| \hat{H} |\Phi\rangle + \hat{H}_N \tag{41}$$

and the expectation value of $\hat{H}$ with respect to the reference state $|\Phi\rangle$ given by

$$\langle\Phi| \hat{H} |\Phi\rangle = \sum_i H_i^i + \frac{1}{2} \sum_{ij} H_{ij}^{ij} + \frac{1}{6} \sum_{ijk} H_{ijk}^{ijk} \ . \tag{42}$$

The normal-ordered Hamiltonian $\hat{H}_N$ again contains a one-body, two-body, and three-body part

$$\hat{H}_N = \hat{H}_N^{[1]} + \hat{H}_N^{[2]} + \hat{H}_N^{[3]} \ , \tag{43}$$

each normal-ordered with respect to the reference state. We denote the normal-ordered k-body part as

$$\hat{H}_N^{[k]} = \frac{1}{(k!)^2} \sum_{p_1,\ldots,p_k} \sum_{q_1,\ldots,q_k} \tilde{H}_{q_1,\ldots,q_k}^{p_1\ldots p_k} \ \{\hat{a}_{p_1}^\dagger \cdots \hat{a}_{p_k}^\dagger \ \hat{a}_{q_k} \cdots \hat{a}_{q_1}\} \ , \tag{44}$$

where the curly brackets enclosing the string of creation and annihilation operators indicates that this product is arranged in normal order with respect to the reference state, i.e., that particle annihilation and hole creation operators are to the right of particle creation and hole annihilation operators. Since the sums over the single-particle indices p_i and q_i run over particle and hole states, the curly brackets indicate that the proper normal order is established for each term of the sum. As a result, we always have $\langle\Phi| \{\hat{a}_p^\dagger \cdots \hat{a}_q\} |\Phi\rangle = 0$ and $\langle\Phi| \hat{H}_N^{[k]} |\Phi\rangle = 0$, in perfect analogy to the relations for the vacuum state $|0\rangle$ in vacuum normal order.

Obviously, we cannot simply change the order of creation and annihilation operators, there are the fermionic anti-commutation relations that we have to obey. Changing the order of creation and annihilation operators produces an extra term, $\hat{a}_p^\dagger \hat{a}_q = \delta_{pq} - \hat{a}_q \hat{a}_p^\dagger$, which has fewer creation and annihilation operators. Starting from a k-body operator (in vacuum normal order) there will be contributions of lower particle ranks in reference normal order, generated by the extra terms. They show up, in the coefficient $\tilde{H}_{q_1,\ldots,q_k}^{p_1\ldots p_k}$ in front of the normal-ordered operators

$$\tilde{H}_q^p = H_q^p + \sum_i H_{qi}^{pi} + \frac{1}{2} \sum_{ij} H_{qij}^{pij} \ , \quad \tilde{H}_{rs}^{pq} = H_{rs}^{pq} + \frac{1}{4} \sum_i H_{rsi}^{pqi} \ , \quad \tilde{H}_{stu}^{pqr} = H_{stu}^{pqr} .$$
$$\tag{45}$$

Working out the commutator algebra manually is a tedious job and can be circumvented by the use of Wick's theorem. We will not go into details here, and rather refer to the literature [61].

As mentioned already, normal ordering is instrumental for the formulation of some many-body methods and we will come back to this in Sect. 6. It can be used

to define in approximation for the multi-nucleon terms in Hamiltonian, specifically for the contribution of the 3N interaction. Looking at the matrix elements in (45) we observe that the three-body contributions H^{pqr}_{stu} of the initial Hamiltonian (in vacuum normal order) enter also into the two-body and one-body part of the reference normal-ordered Hamiltonian. The three-body matrix elements in these terms are partially summed over one or two occupied levels, so effectively selected three-body terms are demoted to lower particle rank. This covers already an important part of the three-body effects and we might omit the residual normal-ordered three-body term in good approximation. This is the so-called normal-ordered two-body (NO2B) approximation [51, 62, 63].

The great advantage of the NO2B approximation is that the many-body method only has to deal with up to two-body terms, which is a significant formal and computational simplification. We can convert the NO2B Hamiltonian back to vacuum normal order and obtain

$$
\hat{H}_{\mathrm{NO2B}} = \frac{1}{6} \sum_{ijk} H^{ijk}_{ijk} + \sum_{pq} \left(H^{p}_{q} - \frac{1}{2} \sum_{ij} H^{pij}_{qij} \right) \hat{a}^{\dagger}_{p} \hat{a}_{q}
$$
$$
+ \frac{1}{4} \sum_{pqrs} \left(H^{pq}_{rs} + \sum_{i} H^{pqi}_{rsi} \right) \hat{a}^{\dagger}_{p} \hat{a}^{\dagger}_{q} \hat{a}_{s} \hat{a}_{r} \, ,
$$
(46)

which can be readily used in many-body methods that do not employ normal ordering otherwise (like, e.g., the no-core shell model).

So far, we have considered a reference state given by a single Slater determinant, a so-called *single-reference* scheme. What about a reference state that is a superposition of multiple Slater determinants? The immediate consequence is that the simple distinction between particle and hole states breaks down. There will be single-particle states that are occupied in some of the determinants making up the reference state and unoccupied in others. Despite this complication, there is a generalization of normal ordering and Wick's theorem [64, 65, 66] for these multi-determinantal reference states, or *multi-reference* states for short. From a practical point of view, the partitioning of the summations into particle and hole states is replaced by unrestricted sums and the information on the structure of the reference state is introduced via density matrices. A more detailed discussion of multi-reference normal ordering and the resulting NO2B approximation can be found in [67].

5 Diagonalization Approaches

After our extensive preparations it is now almost trivial to define a first class of many-body methods. Taking the basis-expansion idea introduced in Sect. 2 literally, we are left with a large-scale matrix eigenvalue problem for the Hamiltonian represented in the A-body basis of choice. The Hamiltonian and the many-body basis make use of the preconditioning methods discussed in the previous section, which are hidden in the A-body matrix elements. This general class of methods is typically identified as

configuration interaction (CI) or exact diagonalization approaches. Methods of this class still differ in the way the many-body basis is truncated and how convergence is assessed.

5.1 Many-Body Truncations

There are different physics-motivated strategies to truncate the many-body basis and to define the many-body model space. Essentially, different truncation schemes define different many-body methods. We discuss the main contenders, provide a physics motivation for the truncation, and comment on uncertainty quantification.

Full Configuration Interaction. Starting from a finite set of single-particle states and building Slater determinants from all possible combinations automatically results in a finite set of A-body basis states spanning the model space of a so-called full configuration interaction (FCI) scheme. In the context of the HO basis, we can use the principal quantum number $e = 2n + l$ to define a single-particle truncation $e \leq e_{max}$ with a control parameter e_{max}. The model space of this FCI scheme can be characterized as

$$\mathcal{M}_{FCI} = \{\text{all Slater determinants } |p_1 p_2 ... p_A\rangle \text{ with } e_{p_i} \leq e_{max}\} . \quad (47)$$

Obviously, in the limit $e_{max} \to \infty$ the FCI calculation will approach the exact result. Therefore, it is in principle straightforward to assess the convergence behavior via an explicit variation of e_{max}. We can derive uncertainty estimates or construct extrapolation schemes to deal with incomplete convergence—all of this is facilitated by the fact that a single parameter, e_{max}, controls the truncation.

This truncation is motivated by the assumption that energetically high-lying single-particle states will contribute less to the basis expansion of low-lying eigenstates. This resonates with the discussion of decoupling of low- and high-energy states in Sect. 4.2. However, the FCI truncation still allows for configurations where all particles occupy the highest available single-particle states—it is very unlikely that such configuration will appear in the expansion of low-lying eigenstates. Not surprisingly, FCI calculations turn out to be rather inefficient in nuclear structure applications.

Particle-Hole-Truncated Configuration Interaction. In addition to the single-particle truncation of FCI we use a truncation on the number of particle-hole pairs that distinguish a basis state from a specific reference state $|\Phi\rangle$. The reference state represents a specific basis determinant, typically the one with the A energetically lowest single-particle states occupied and can be obtained, e.g., from an HF calculation. All basis states can be classified according to the number of single-particle states that differ from the reference state $|\Phi\rangle$. Or, equivalently, the number of particle-hole excitations needed to construct a basis determinant from the reference state.

We can use the creation and annihilation operators of second quantization to define n-particle-n-hole (npnh) excitations on top of the reference state $|\Phi\rangle$:

$$
\begin{aligned}
\text{1p1h}: \quad & |\Phi_i^a\rangle = \hat{a}_a^\dagger \hat{a}_i |\Phi\rangle \\
\text{2p2h}: \quad & |\Phi_{ij}^{ab}\rangle = \hat{a}_a^\dagger \hat{a}_b^\dagger \hat{a}_j \hat{a}_i |\Phi\rangle \\
\text{3p3h}: \quad & |\Phi_{ijk}^{abc}\rangle = \hat{a}_a^\dagger \hat{a}_b^\dagger \hat{a}_c^\dagger \hat{a}_k \hat{a}_j \hat{a}_i |\Phi\rangle \, ,
\end{aligned}
\tag{48}
$$

where we again use the index convention with i, j, k being hole states that are occupied in the reference state and a, b, c particle states that are unoccupied in $|\Phi\rangle$. This hierarchy can be easily extended to the A-particle-A-hole level.

Including all levels of this particle-hole hierarchy will simply recover the FCI model space, we have only structured the basis in a physically useful manner. However, we can introduce an additional, physics motivated truncation by only keeping basis states up to a specific maximum npnh level and, thus, define the npnh-truncated model space of CI(npnh)

$$
\begin{aligned}
\mathcal{M}_{\text{CI}(n\text{p}n\text{h})} = \{&\text{all Slater determinants } |\Phi\rangle, |\Phi_i^a\rangle, |\Phi_{ij}^{ab}\rangle, ... \\
&\text{up to the } n\text{p}n\text{h level with } e_{a,b,...} \leq e_{\max}\} \, .
\end{aligned}
\tag{49}
$$

Note that we still need the $e_{\max}$ truncation, since the particle-hole truncation alone would not render the model space finite. Thus, we have to handle two parameters that control the truncation of the model space, n and $e_{\max}$. This makes the study of the convergence as well as the quantification of uncertainties more difficult, particularly since the inclusion of the next particle-hole level typically increases the model-space dimension by orders of magnitude.

The physics motivation behind the particle-hole hierarchy results from a perturbative consideration. We can consider the reference state as a simple first approximation for the ground state of our system—very much in the spirit of HF—and, thus, as the lowest-order approximation in a perturbative expansion. The first-order perturbative corrections to this state will only include up to 2p2h excitations on top of $|\Phi\rangle$ if the Hamiltonian contains up to two-body operators. This is because the amplitudes of the perturbative correction to the states involve matrix elements $\langle\Phi_{ij...}^{ab...}|\hat{H}|\Phi\rangle$, which vanish beyond the 2p2h level. Second-order corrections to the many-body states will include up to 4p4h excitations etc. Thus, multi-particle-multi-hole states enter in increasing orders of perturbation theory, and we expect their contribution to be increasingly suppressed.

So far, we have considered the simple situation of a closed-shell system, which is characterized by a unique Slater determinant as a reference state. For an open-shell system, the filling of single-particle states in energetic order results in a partially occupied j-orbit, i.e., not all $(2j + 1)$ magnetic substates are filled. As a result, there are multiple possible reference Slater determinants with the same total unperturbed energy—there is a set of degenerate reference states. This trivial effect has huge consequences, it is at the heart of all the differences between single-reference (closed-shell) and much more complicated multi-reference (open-shell) methods that

will be discussed later. At the moment, we are only interested in model-space trun-
cations in a CI framework and there is an easy fix. Instead of counting particle-hole
excitations with respect to a specific reference state, which will depend on which of
the degenerate reference states we have picked, we count the single-particle states
that are above the last (partially) occupied orbit of the degenerate reference states.
This truncation is sometimes called T_{max} truncation, where T is the number of single-
particle states above the last reference orbit. When applied in a closed-shell situation,
the T_{max} truncation is equivalent to an $npnh$-truncation with $n = T_{max}$.

No-Core Shell Model. The previous CI truncations are used across different fields
of quantum physics and quantum chemistry. The truncation we are discussing now,
which defines the so called no-core shell model (NCSM), is more specific to nuclear
physics [68, 69]. In its pure version, the NCSM uses an HO single-particle basis in
combination with a truncation with respect to the total HO energy of the many-body
basis states. This total HO energy is parametrized in terms of a parameter N_{max},
which counts the HO excitation quanta above the lowest-energy HO determinant,
i.e., the reference state. Formally, the number of excitation quanta N is obtained from

$$N = \sum_{i=1}^{A} e_i - E_{ref}. \qquad \text{with} \qquad E_{ref} = \sum_{i=1}^{A} e_i^{ref} , \qquad (50)$$

where E_{ref} is the total principal quantum number of the lowest-energy reference
configuration whose single-particle state have principal quantum numbers e_i^{ref}. Note
that degeneracy of reference determinants in the case of open-shell systems does not
pose a problem here. For the HO basis the number of excitation quanta N can be
translated into an HO excitation energy by multiplying with $\hbar\Omega$. The NCSM model
space is, thus, defined as

$$\mathcal{M}_{NCSM} = \{\text{all Slater determinants } |p_1 p_2 ... p_A\rangle \text{ with } N \leq N_{max}\} . \qquad (51)$$

Like the FCI scheme, the NCSM model space is based on a truncation with respect to
an unperturbed energy. However, the NCSM uses the total energy of the many-body
basis state, not the single-particle energy. Therefore, high-energy configurations with
all particles in high-lying single particle states are excluded.

   Again, we can resort to perturbation theory to motivate this energy truncation.
Looking at the corrections to the many-body state predicted in perturbation theory,
the contributions of individual states are always scaled by energy denominators,
which correspond exactly to the HO excitation energies $N\hbar\Omega$. Thus, with increasing
N the contribution of configurations gets more and more suppressed by the energy
denominators. The N_{max} truncation, therefore, discards configurations that are ex-
pected to have small contributions based on a perturbative estimate. In this sense,
the N_{max} truncation is much more physics-driven than the simple e_{max} truncation.

   Nowadays, the NCSM truncation is also used with other single-particle basis sets
than the HO, for example the natural orbitals discussed in Sect. 4.3.3. In this case, the
N_{max} parameter looses its direct connection to the unperturbed energies and is purely
defined on the basis of a pseudo-principal quantum number $e = 2n + l$. Nevertheless,

it remains a useful and efficient truncation, as the gross picture of energy scales is still valid. Since the NCSM is the main work horse among the ab initio CI methods in nuclear physics, we will come back to it in Sect. 5.3.

Valence-Space Shell Model. Also the traditional valence-space shell model (VSSM) of nuclear physics can be viewed as a specific incarnation of the general configuration interaction idea. It is based on a partitioning of the single-particle basis into three subsets: core states, valence states, and excluded sates. The many-body basis is then characterized by two different truncations: (1) a simple single-particle truncation that eliminates all the excluded single-particle states; (2) a selective truncation that retains only many-body configurations that have all core states filled. As a result, the basis configurations of the many-body model space all have A_c nucleons occupying the same A_c core states, and the states only differ in the assignments of the $A_v = A - A_c$ remaining valence nucleons to the valence single-particle states. We can summarize the VSSM model space as follows

$$\mathcal{M}_{\text{VSSM}} = \{\text{all Slater determinants } |p_1 p_2 ... p_A\rangle \text{ with} \\ \{p_1, ..., p_{A_c}\} = \text{core and } \{p_{A_c+1}, ..., p_A\} \subset \text{valence space}\} . \tag{52}$$

For shell-model practitioners this definition might sound unfamiliar. Practical VSSM calculations do not work with an A-body Slater determinant basis, but with an A_v-body basis of the same dimension. Since the same core states are occupied in all basis states of the model space, their contribution to all relevant many-body matrix elements can be computed beforehand and absorbed into the remaining valence-space part of the matrix elements. This is a purely technical step akin to the normal ordering of operators discussed in Sect. 4.4. The reduction to an effective A_v-body problem does not imply additional approximations, it is an equivalent reformulation of the problem.

Although the VSSM can be viewed as a truncation of the A-body Hilbert space, its practical applications follow a different philosophy than the other CI-type approaches. In all ab initio CI approaches, the truncation parameters are varied in order to assess the convergence towards the full Hilbert space and to extract model-space uncertainties. This is not done in typical VSSM calculations that work with a fixed valence space that is governed by computational feasibility and not by convergence considerations. In practice, a systematic variation of core and excluded space is often not possible, as model space dimensions become intractable very quickly. Therefore, VSSM calculations are traditionally performed in a phenomenological setting, with valence space interactions fitted to nuclear observables, e.g., excitation energies, for nuclei in the respective valence shell. For other observables, e.g., electromagnetic transition strengths and moments, phenomenological corrections in the form of effective charges are introduced. In addition to purely phenomenological interactions, effective interactions derived in a perturbative framework or in a decoupling scheme are being used. In this way, the connection to the underlying Hamiltonian is retained, however, a quantification of model-space uncertainties generally is still lacking.

Symmetry Reduction. For all the truncations discussed so far, we can take into account symmetries to further reduce the basis dimension. The most important symmetries for our purpose are charge conservation and rotational invariance.

As a consequence of charge conservation, the number of protons and neutrons is fixed and, thus, the total isospin projection $M_T = Z - N$ is a good quantum number of the nuclear eigenstates. In technical terms, there is a simultaneous eigenbasis of the Hamiltonian and the operator $\hat{T}_3 = \sum_i \hat{t}_{3,i}$ for the 3-component of the total isospin. The Slater determinant basis states that span the CI model spaces are also eigenstates to $\hat{T}_3$ and the eigenvalue is the sum of all single-particle isospin projections m_t, cf. eq. (2). Therefore, only basis states with appropriate M_T contribute to the expansion of the eigenstates and we can discard all other basis states from the model space. Obviously, this is a simple and effective way to reduce the model-space dimension without changing the results.

A similar argument applies to the projection M of the total angular momentum $\hat{J}_z = \sum_i \hat{j}_{z,i}$. Due to the rotational symmetry of the problem, the Hamiltonian does not connect states with different M quantum numbers and the energy spectrum exhibits a degeneracy with respect to M. Therefore, we can choose a specific value of M at the beginning of the calculation and only include basis states with this specific M into the model space. Again, the Slater determinant states are also eigenstates to $\hat{J}_z$ with eigenvalues given by the sum of the single-particle projections m.

One could consider going one step further with rotational symmetry. The Hamiltonian also commutes with the square of the total angular momentum operator $\hat{\mathbf{J}}^2$, therefore, J is also a good quantum number for the nuclear eigenstates. We could focus on a specific value of J and limit the model space to basis states with this value of J. The problem here is that Slater determinants are generally not eigenstates of $\hat{\mathbf{J}}^2$, therefore, a simple basis-state selection is not possible. One can, however, use information on a specific target value for J through the choice of M. Usually one uses $M = 0$ (for even A) or $M = \frac{1}{2}$ (for odd A), because this is compatible with all possible J values. For targeting larger values of J, one can use $M = J$, which will reduce the model-space dimension but exclude all eigenstates with $J < M$.

In order to exploit the good J quantum number, one has to use a J-coupled basis. The construction of such a basis is much more involved than the simple Slater determinant basis and the computation of many-body matrix elements is far from trivial. Therefore, J-coupled basis sets are rarely used in the CI context. Exceptions are J-scheme versions of the valence-space shell model and Jacobi-coordinate version of the NCSM.

A final remark: One can approach the question of symmetries from a completely different angle. Instead of trying to incorporate the good quantum number into the basis to reduce the model-space dimension, one can break symmetries on purpose to enrich the basis and include specific correlations, and later restore the broken symmetries explicitly in order to arrive at the nuclear eigenstate. This symmetry breaking and restoration strategy is particularly helpful to describe collective correlations, also called static correlations, such as the intrinsic deformation of a nucleus.

5.2 Importance Truncation

All ab initio CI approaches are eventually limited by the trade-off between convergence and model-space dimension. The model space has to be large enough to reach acceptable convergence of the target observable, but the computational cost for the calculation increases rapidly with model-space size. With increasing particle number A one quickly faces the situation that the calculation cannot be converged with numerically tractable basis dimensions. However, there is one more trick—the selective removal of basis states from the model space using an adaptive, state-specific, and physics-guided truncation criterion [70, 71].

Assume we target a small number of low-lying eigenstates $|\Psi^{(m)}\rangle$ for $m = 1, ..., M$ in a CI calculation for a specific model space. The full calculation would yield eigenvectors representing the amplitudes $C_\nu^{(m)}$ for the expansion of the target eigenstates in terms of the many-body basis states $|\Phi_\nu\rangle$:

$$|\Psi^{(m)}\rangle = \sum_\nu C_\nu^{(m)} |\Phi_\nu\rangle \; . \tag{53}$$

Many of the amplitudes will be very small or vanishing, i.e., the corresponding basis states do not contribute significantly to the target states. If these amplitudes were known beforehand, we could reduce the basis dimension significantly by discarding those basis states.

In order to estimate the amplitudes a priori, we use initial approximations of the target states, the reference states $|\Psi_{\text{ref}}^{(m)}\rangle$, that are typically determined from a previous CI calculation in a smaller model space $\mathcal{M}_{\text{ref}}$

$$|\Psi_{\text{ref}}^{(m)}\rangle = \sum_{\nu \in \mathcal{M}_{\text{ref}}} C_{\text{ref},\nu}^{(m)} |\Phi_\nu\rangle \; . \tag{54}$$

These reference states carry information about the physical properties of the target eigenstates. Guided by first-order multiconfigurational perturbation theory, we estimate the amplitudes of the individual basis states $|\Phi_\nu\rangle \notin \mathcal{M}_{\text{ref}}$ in the expansion of the target eigenstate [71]. This first-order perturbative correction for the amplitudes defines the so-called importance measure

$$\kappa_\nu^{(m)} = -\frac{\langle \Phi_\nu | \hat{H} | \Psi_{\text{ref}}^{(m)} \rangle}{\Delta\epsilon_\nu} \; , \tag{55}$$

where $\hat{H}$ is the full Hamiltonian and $\Delta\epsilon_\nu$ is the unperturbed HO excitation energy of the basis state $|\Phi_\nu\rangle$ [70, 71].

The importance measure combines information about the properties of the target states, carried by the reference states, about the many-body basis, and about the Hamiltonian. It is the foundation for the definition of a state-dependent adaptive truncation of the model space, the so-called importance truncation (IT). We define the importance-truncated model-space $\mathcal{M}_{\text{IT}}(\kappa_{\text{min}})$ spanned by all states of the reference

space $\mathcal{M}_{\text{ref}}$ plus all basis states $|\Phi_\nu\rangle \notin \mathcal{M}_{\text{ref}}$ with importance measure $|\kappa_\nu^{(m)}| \geq \kappa_{\text{min}}$ for at least one $m \in \{1, ..., M\}$. The importance threshold κ_{min} provides an additional truncation parameter, which will be varied later on to probe the contribution of the discarded basis states. Note that the importance measure (55) is based on the first-order perturbative correction to the states, not on the perturbative correction to the energies. It is, therefore, not biased to an optimal description of energies, but aims at an optimal description of the states and, thus, of all observables.

Depending on the specific flavour of CI, we can use different strategies to set up the importance-truncated model space. We can use iterative schemes, where the IT-space is successively refined and expanded by using improved reference states from a previous IT calculation. For the NCSM a particularly efficient scheme uses the eigenstate of the next smaller N_{max} as reference state for the construction of the IT model space.

The importance threshold κ_{min} acts as an additional truncation parameter of the CI model space, and it is guaranteed that in the limit $\kappa_{\text{min}} \to 0$ we recover the original CI model space. In practical applications, we typically perform calculations for a sequence of importance thresholds κ_{min} and use an extrapolation of the observables to vanishing importance threshold to effectively account for discarded basis states. More details on the practical aspects of IT calculations can be found in [71, 72].

5.3 No-Core Shell Model

Since the NCSM is the most commonly used ab initio CI method in nuclear structure physics [68, 69], we will discuss the main components of the calculation and illustrate the convergence behavior in a little more detail.

Setup and numerics. As discussed before, the NCSM uses a basis build from HO single-particle states and is truncated with respect to the maximum number of HO excitation quanta N_{max}. This model space has the unique advantage that the center-of-mass motion can be separated or factorized exactly from the intrinsic state of the system. Therefore, we can use simple tricks like adding an extra HO Hamiltonian for the center-of-mass to remove spurious center-of-mass excitations from the low-lying excitation spectrum. This model space also offers two alternative basis sets to work with: the Slater determinant HO basis and the relative-coordinate or Jacobi HO basis, mentioned in Sect. 4.3.1. The former defines the standard m-scheme NCSM, which is more universal and applicable to heavier nuclei, and the latter the Jacobi NCSM, which is very efficient for light nuclei with $A \lesssim 6$ [73]. The standard NCSM has the advantage of numerical simplicity, e.g., for the computation of matrix elements, but it requires large basis dimensions. The Jacobi NCSM can realize much smaller basis dimensions for the same N_{max}, because all symmetries, including translational and rotational invariance, are exploited, however, the computation of matrix elements is much more complicated and practically feasible only for light nuclei.

Let us expand on the computational aspects of standard NCSM calculations in large model spaces. Today, advanced NCSM implementations handle model spaces

with up to 10^{10} basis states [74, 75], i.e., they tackle the eigenvalue problem of a $10^{10} \times 10^{10}$ matrix, which might seem impossible. Storing this full matrix with single-precision floating-point numbers would require on the order of 10^8 TB of storage. Luckily, the Hamilton matrix is very sparse, and we only need to store the non-zero matrix elements. This is because a Hamiltonian with up to two or three-body interactions connects only those pairs of basis states that differ by up to two or three single-particle states, respectively. As a result, the sparsity decreases with increasing particle-rank of the Hamiltonian, which is why the NO2B approximation discussed in Sect. 4.4 can be useful in the NCSM as well.

These huge basis sizes require an efficient computation of many-body matrix elements—a significant fraction of the total runtime goes into the computation of the matrix elements of the Hamiltonian. The next step in the calculation is the solution of the matrix eigenvalue problem. Since we are only interested in a tiny fraction of the eigenstates at the lower end of the spectrum, we can use iterative Krylov subspace methods, like the famous Lanczos or Arnoldi algorithms. Each iteration of these algorithms requires a matrix-vector multiplication, which can be implemented efficiently with sparse matrix storage and even with distributed memory schemes. Only about 10 iterations are needed to converge the lowest eigenvalue, i.e., the ground state, and for about 100 iterations we typically get the interesting part of the low-lying excitation spectrum. If the matrix elements are computed very efficiently, one can even consider computing them on-the-fly during the evaluation of matrix-vector products without ever storing them—this shifts characteristics of the calculation from being very storage intensive to being very compute intensive.

As for all CI methods, the solution of the eigenvalue problem yields the energies of the low-lying states and the eigenvectors that contain the coefficients for the basis expansion of the eigenstates in Eq. (5). They can be used in a post-processing step to evaluate all other observables that are defined in terms of expectation values or matrix elements with these eigenstates. Note that ground and excited states are always obtained on the same footing.

Convergence and frequency dependence. The model-space size is controlled solely by the truncation parameter $N_{\max}$ and we recover the full Hilbert space in the limit $N_{\max} \to \infty$. The HO basis has an additional parameter, the oscillator frequency $\hbar\Omega$, and all observables have to become independent of $\hbar\Omega$ in the limit of large $N_{\max}$. However, the choice of $\hbar\Omega$ will affect the convergence behavior of the calculation. An example for NCSM calculations with the HO basis is shown in the left-hand panels of Fig. 2 for the ground-state energy and the point-proton rms radius of ^{16}O. The observables are plotted as function of $\hbar\Omega$ with different curves representing different $N_{\max}$. For the ground state energy we observe the characteristic monotonic convergence from above—the curves shift downwards and flatten out with increasing $N_{\max}$. For the rms-radii the convergence pattern is completely different, there is no variational principle that warrants monotonic convergence and we observe that, depending on $\hbar\Omega$, the radius converges from above or below. For both observables there are sweet-spots in $\hbar\Omega$ which yield the most rapid convergence. For the energy this is in the range of $\hbar\Omega = 16$ to 20 MeV and for the rms-radius at 16
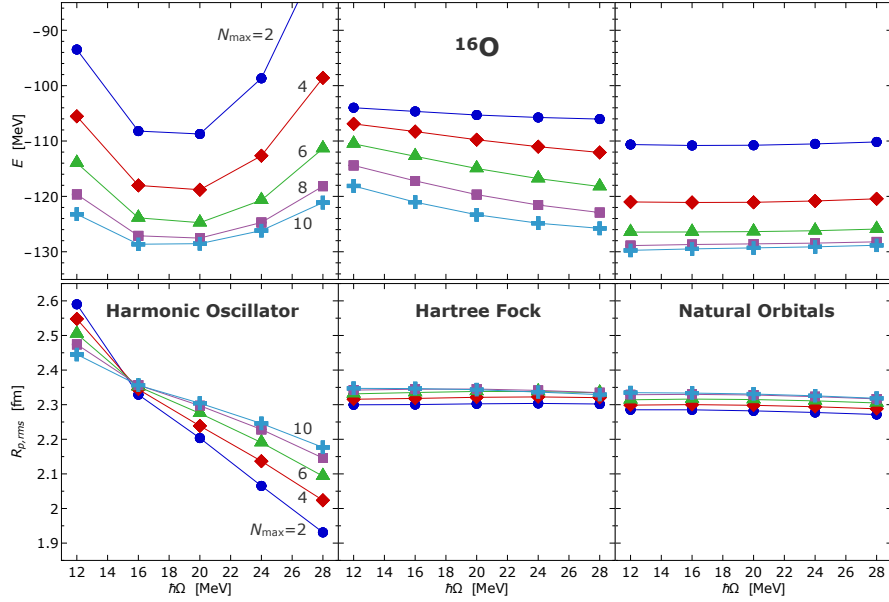
Fig. 2 Comparison of the convergence of NCSM calculations with three different basis sets for the ground-state energy and point-proton rms-radius for ^{16}O using an SRG-evolved chiral NN+3N interaction with $\alpha = 0.08\,\mathrm{fm}^4$. Modified from [60].

MeV, where the radius is practically independent of N_{max}. We can use these optimal values of $\hbar\Omega$ to extract a most converged result and possibly even improve on it via an extrapolation $N_{\mathrm{max}} \to \infty$ with quantified uncertainties. This shows, however, that we have to perform NCSM calculations for multiple values of $\hbar\Omega$ to explore the frequency dependence of each observable.

Basis optimization. What does the convergence look like with the other single-particle basis sets? Of course, with the HF and the natural-orbital states discussed in Sect. 4.3 we loose the formal properties of the HO, e.g., the exact separation of intrinsic and center-of-mass degrees of freedom. We also do not have the equidistant energy spectrum and the interpretation of $N_{\mathrm{max}}\hbar\Omega$ as unperturbed excitation energy anymore, but we can still set up an N_{max}-truncated model space based on the quantum numbers of the single-particle states, using the pseudo-principal quantum number $e = 2n + l$ th evaluate N_{max}. As discussed in Sect. 4.3 we still use the HO to represent the single-particle states of these optimized basis sets, therefore, there is still an $\hbar\Omega$ parameter involved.

The NCSM results for ^{16}O with the HF and the natural-orbital basis are depicted in the center and right-hand columns of Fig. 2. The convergence of the ground-state energy with the HF basis shows an anomalous pattern: the frequency dependence is reduced but the energies drop almost linearly with N_{max} and the $N_{\mathrm{max}} = 10$ results are
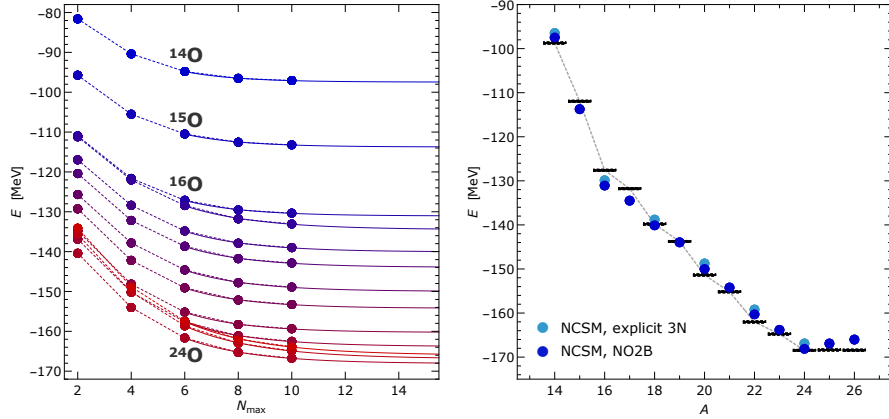
Fig. 3 NCSM calculations for the ground-state energies of oxygen isotopes. Left: Convergence of the energy as function of N_{max} using the natural orbital basis together with an exponential extrapolation. Right: Extrapolated ground-state energies obtained with the full 3N interaction and with the NO2B approximation in comparison to experiment.

well above the corresponding HO energies. This is related to the pathologies of the HF basis discussed in Sect. 4.3.2, which is not not suitable for NCSM calculations.

The situation is different with the natural-orbital basis. As evident from the right-hand panels of Fig. 2 energies and radii are, for all practical purposes, independent of $\hbar\Omega$. The N_{max}-convergence of both observables is comparable to the convergence with the HO basis for the optimal $\hbar\Omega$. This is a great result! We do not need to optimize $\hbar\Omega$ anymore, this is done implicitly by the natural orbitals already, because it contains global information on the nucleus, such as its size.

Oxygen isotopic chain. Using the natural-orbital basis, we can attempt large-scale NCSM calculations that reach the limit of particle numbers the NCSM can handle. We consider the oxygen isotopic chain from the neutron deficient ^{14}O to ^{26}O beyond the neutron dripline and the results are summarized in Fig. 3. Because of the preconditioning, using the natural-orbital basis with an SRG-evolved Hamiltonian, we are close to convergence for $N_{max} = 10$ and simple exponential extrapolations can be used to obtain a final energy with an uncertainty estimate. Reaching these large N_{max} parameters for $A \approx 20$ systems requires the IT scheme discussed in Sect. 5.2. The right-hand panel of Fig. 3 shows the extrapolated ground-state energies for calculations with explicit 3N terms in the Hamiltonian in comparison to the NO2B approximation. We observe a small overestimation of the ground state energy by $1 - 2$ MeV when using the NO2B approximation, which is acceptable given that the NCSM calculation speeds up by a factor of 10 due to the increased sparsity of the Hamilton matrix.

For going much beyond the oxygen isotopes, we have to resort to a different many-body strategy—we will move from diagonalization to decoupling.

6 Decoupling Approaches

We have already established the conceptual relation between *diagonalization* and *decoupling* during the discussion of unitary transformation and the SRG in Sect. 4.2. Now we transfer this directly to the methods for the solution of the many-body problem. The CI approaches discussed in the previous section use the concept of diagonalization—we construct a matrix representation of the Hamiltonian and solve the matrix eigenvalue problem, which is equivalent to a diagonalization of the matrix. Typically we will only extract a few low-lying eigenvalues and eigenvectors, which can be viewed as a selective diagonalization of a few rows and columns of the matrix. This structure of the matrix could also be viewed as a specific decoupling, i.e., a suppression of the off-diagonal matrix elements that connect the low-lying states with the rest of the model space.

6.1 In-Medium Similarity Renormalization Group

The most obvious implementation of the decoupling strategy is the SRG framework discussed in Sect. 4.2. We can use the SRG flow-equation to drive a continuous decoupling of a selected state or subspace from the rest of the model space. In contrast to the free-space SRG, we now aim at a pre-diagonalization of the Hamiltonian in A-body space. As mentioned earlier, the direct solution of the flow equations for the Hamiltonian in an A-body CI-type matrix representation is neither advantageous nor feasible. Therefore, we combine the SRG flow-equation with the normal-ordering of the Hamiltonian and a truncation analogous to the NO2B approximation discussed in Sect. 4.4. This results in the so-called in-medium similarity renormalization group (IM-SRG) [76, 77, 78, 79, 80].

Let us start with the single-reference formulation of normal ordering suitable for closed shell nuclei. We define a reference state $|\Phi\rangle$ as a single Slater determinant constructed, e.g., in a previous HF calculation or with a natural-orbital basis. We convert the relevant operators for the formulation of the SRG flow equation into normal-ordered form with respect to this reference state and truncate after the normal-ordered two-body terms, i.e., the Hamiltonian

$$\hat{H}(s) = E(s) + \sum_{pq} H_q^p(s) \{\hat{a}_p^\dagger \hat{a}_q\} + \frac{1}{4} \sum_{pqrs} H_{rs}^{pq}(s) \{\hat{a}_p^\dagger \hat{a}_q^\dagger \hat{a}_s \hat{a}_r\} \ . \qquad (56)$$

and the anti-hermitean generator

$$\hat{\eta}(s) = \sum_{pq} \eta_q^p(s) \{\hat{a}_p^\dagger \hat{a}_q\} + \frac{1}{4} \sum_{pqrs} \eta_{rs}^{pq}(s) \{\hat{a}_p^\dagger \hat{a}_q^\dagger \hat{a}_s \hat{a}_r\} \ . \qquad (57)$$

The Hamiltonian, the generator, and all their matrix elements are functions of the IM-SRG flow parameter s (we reserve α for the free-space SRG flow parameter).

The zero-body part of the Hamiltonian, i.e. the expectation value of the Hamiltonian in the reference state, is denoted by $E(s)$. These normal-ordered operators enter in the IM-SRG flow equation, which looks just like the general SRG flow equation (18)

$$\frac{\mathrm{d}}{\mathrm{d}s}\hat{H}(s) = \left[\hat{\eta}(s), \hat{H}(s)\right] \ . \tag{58}$$

After working out the commutator with normal-ordered operators and truncating again after the two-body level, we obtain a system of coupled first order differential equations for the normal-ordered zero-body, one-body, and two-body matrix elements of the Hamiltonian

$$\frac{\mathrm{d}}{\mathrm{d}s}E = \sum_{pq}\eta_q^p H_p^q (n_p - n_q) + \frac{1}{2}\sum_{pqrs}\eta_{rs}^{pq} H_{pq}^{rs} n_p n_q \bar{n}_r \bar{n}_s$$

$$\frac{\mathrm{d}}{\mathrm{d}s}H_2^1 = \sum_{p}\left[\eta_p^1 H_2^p + (1 \leftrightarrow 2)\right] + \sum_{pq}(n_p - n_q)\left(\eta_q^p H_{p2}^{q1} - H_q^p \eta_{p2}^{q1}\right)$$

$$\qquad + \frac{1}{2}\sum_{pqr}\left[\eta_{pq}^{r1} H_{r2}^{pq}(n_p n_q \bar{n}_r + \bar{n}_p \bar{n}_q n_r) + (1 \leftrightarrow 2)\right]$$

$$\frac{\mathrm{d}}{\mathrm{d}s}H_{34}^{12} = \sum_{p}\left[\eta_p^1 H_{34}^{p2} - H_p^1 \eta_{34}^{p2} - (1 \leftrightarrow 2)\right] - \sum_{p}\left[(\eta_3^p H_{p4}^{12} - H_3^p \eta_{p4}^{12}) - (3 \leftrightarrow 4)\right]$$

$$\qquad + \frac{1}{2}\sum_{pq}\left[\eta_{pq}^{12} H_{34}^{pq}(1 - n_p - n_q) + (1,2 \leftrightarrow 3,4)\right]$$

$$\qquad - \sum_{pq}(n_p - n_q)\left[(\eta_{p4}^{q2} - \eta_{q3}^{p1} H_{p4}^{q2}) - (1 \leftrightarrow 2)\right] \ , \tag{59}$$

where we have omitted the flow-parameter arguments for brevity. We have introduced single-particle occupation numbers $n_p \in \{0, 1\}$ and $\bar{n}_p = 1 - n_p$ of the reference state to effectively distinguish hole and particle states. Note that the external single-particle indices that enter on the left-hand side are simply denoted by numbers to easily distinguish them from the additional summation indices.

We have not specified the generator $\hat{\eta}(s)$ yet, but we can draw on our discussion in Sect. 4.2. The simplest choice for $\hat{\eta}(s)$ is again the Wegner ansatz (19)

$$\hat{\eta}_{\mathrm{W}}(s) = [\hat{H}^d(s), \hat{H}(s)] = [\hat{H}^d(s), \hat{H}^{od}(s)] \tag{60}$$

with a commutator of the diagonal parts $\hat{H}^d(s)$ and off-diagonal parts $\hat{H}^{od}(s)$ of the Hamiltonian. The Wegner generator is not very efficient, and in practical applications other choices, mainly the imaginary-time and White generators, are being used. We refer to the literature for more details [78, 79, 80]. For all generators we still have to decide what we consider as diagonal and off diagonal, this defines the decoupling pattern.
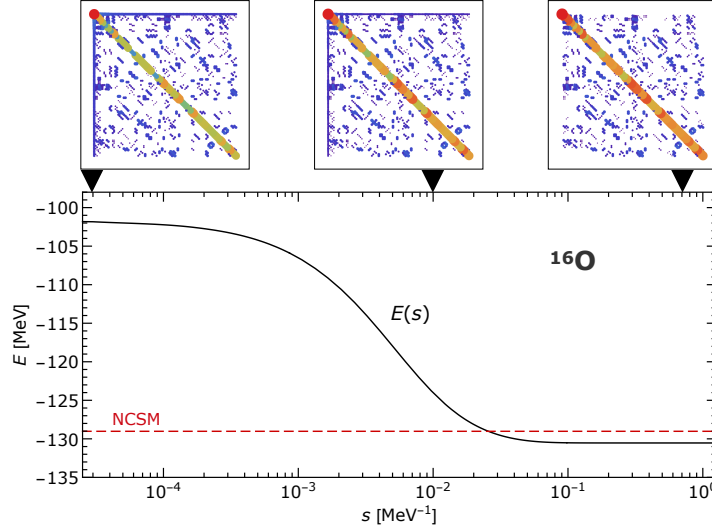
Fig. 4 Illustration of an IM-SRG evolution for ^{16}O. The bottom panel shows the flow-parameter dependence of the zero-body part $E(s)$ of the Hamiltonian in comparison to the NCSM result for the ground state energy. The upper panels depict a part of the evolved Hamiltonian in a particle-hole basis representation for different values of s. Each circle indicates a non-vanishing matrix element and its area encodes the absolute value of the matrix element.

The single-reference IM-SRG for closed-shell nuclei uses a simple and extreme decoupling pattern. The off-diagonal part of the Hamiltonian is everything that connects the reference state $|\Phi\rangle$ to any other basis state. In the language of the matrix elements $H_p^q(s)$ and $H_{pq}^{rs}(s)$, all matrix elements that connect particle and hole states are considered off-diagonal. Consequently the IM-SRG aims to decouple the reference state from all particle-hole excitations. This is illustrated with an actual IM-SRG evolution for ^{16}O in Fig. 4. The top row depicts matrix representations of the Hamiltonian in a particle-hole CI basis with increasing flow parameters marked by triangles. The flow evolution will selectively diagonalize the matrix with respect to the first row and column with the matrix element $\langle\Phi|\hat{H}(s)|\Phi\rangle$ on the diagonal. The lower panel shows the evolution of this matrix element, which constitutes zero-body part of the flowing Hamiltonian $E(s) = \langle\Phi|\hat{H}(s)|\Phi\rangle$. With increasing flow parameter, $E(s)$ first decreases and then stabilizes once the decoupling is achieved. In this decoupled regime, $E(s)$ corresponds to an eigenvalue and directly represents the ground-state energy of the system.

Addressing other ground-state observables, e.g., the rms-radius, requires more work. As discussed in Sect. 4.2.2, we have to transform the matrix elements of the observable consistently using the same IM-SRG flow evolution. At this point the Magnus formulation of the flow equations comes in handy (cf. Sect. 4.2.2) and is used in many state-of-the-art IM-SRG implementations.

The numerical character of IM-SRG calculations is very different from the CI or NCSM approaches discussed before. We are dealing with an initial value problem for a system of coupled first-order differential equations (59) for the matrix elements of the normal-ordered Hamiltonian. Similar to FCI, the single-particle basis has to be truncated to arrive at a finite set of equations. Beyond the m-scheme formulation discussed here, we can use angular momentum coupled matrix elements and exploit their symmetries in order to reduce the number of equations drastically. In this way, large single-particle basis sets become tractable with moderate computational effort. Note that the particle number A does not directly affect the dimension of the system of differential equations (59), so heavy nuclei are accessible in principle.

A final comment regarding uncertainties: Multiple truncations are being used in the IM-SRG framework: the truncation of the single-particle basis, the NO2B approximation of the initial Hamiltonian, the NO2B truncation of commutator terms leading to the flow equations, and further truncations at the level of the 3N matrix elements entering the calculation. All these truncation potentially affect the results and it is difficult to quantify them explicitly within the IM-SRG method. Therefore, comparisons with other many-body approaches, e.g., the NCSM as shown in Fig. 4, are important to gauge the accuracy.

6.2 In-Medium No-Core Shell Model

The single-reference IM-SRG formulation is rather limited, we would certainly like to address excited states and open-shell nuclei as well in an IM-SRG framework. One option is to use the single-reference IM-SRG formulation in conjunction with the VSSM [81, 82]. Here the IM-SRG is used to decouple the valence space from the closed-shell core and from the excluded space. This approach has been used successfully in a range of different applications, but it inherits the limitations of the VSSM discussed in Sect. 5.1.

A more powerful option is the use of a multi-reference formulation of the IM-SRG. It results from the combination of the SRG flow equations with multi-reference normal ordering, mentioned in Sect. 4.4. Instead of being limited to single-determinant reference states, we can now use much more elaborate reference states, tailored for open-shell situations. The first formulation of a multi-reference IM-SRG approach employed reference states from particle-number projected Hartree-Fock-Bogoliubov calculations, which give access to semi-magic isotopic chains [83, 84]. However, we can go further than this and combine the multi-reference IM-SRG with reference states from the NCSM. This will lead to a new hybrid ab initio method, the in-medium no-core shell model (IM-NCSM) [85].

We will not go into the equations for the general multi-reference IM-SRG but refer to the literature [80, 85]. Compared to the single-reference equations (59) the information on the reference states is encoded in density matrices in addition to the occupation numbers, which directly result from the multi-reference normal-ordering. For the IM-NCSM we use an NCSM eigenstate for a small model space, typically
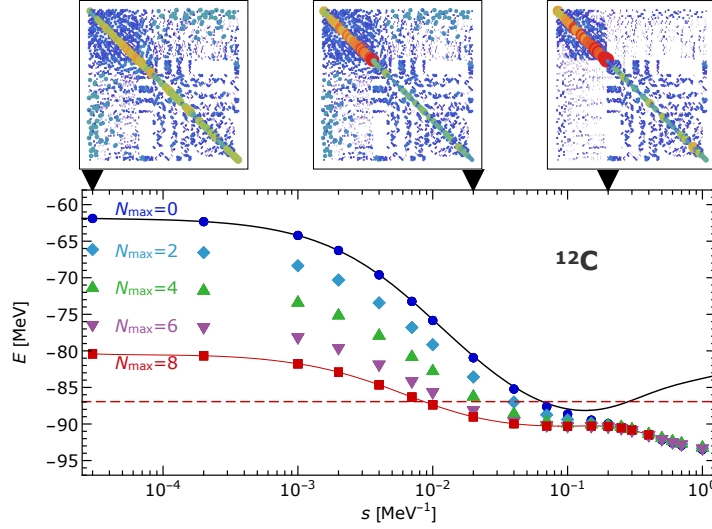
Fig. 5 Illustration of an IM-NCSM evolution for ^{12}C. The bottom panel shows the flow-parameter dependence of the zero-body part $E(s)$ as well as NCSM results for the ground-state energy obtained with the evolved Hamiltonian in different model spaces. The upper panels depict a part of the evolved Hamiltonian in an NCSM basis representation for different values of s. Each circle indicates a non-vanishing matrix element and its area encodes the absolute value of the matrix element.

$N_{max} = 0$ or 2 as reference state. The reference state already contains a significant amount of correlations and we control the complexity of the reference state through the size of the model or reference space the state is obtained from. Since we will be using an angular momentum coupled formulation of the multi-reference flow equations, we will limit ourselves to reference states with $J = 0$ leading to scalar density matrices.

The multi-reference IM-SRG flow evolution will decouple the reference space from the rest of the model space. This is illustrated in Fig. 5 showing the flow evolution for ^{12}C with an $N_{max}^{ref} = 0$ reference space. The upper panels depict a part of Hamiltonian in the NCSM many-body basis at different flow parameters. The upper-left corner of the matrix shows the $N = 0$ sector of the matrix, the rest belongs to the $N = 2$ subspace. We observe that the $N = N_{max}^{ref} = 0$ block is decoupled from the rest of the model space throughout the flow evolution, i.e., the off-diagonal blocks are suppressed. As a result of the IM-SRG evolution we obtain an approximately block-diagonal Hamiltonian, which serves as import for a second NCSM calculation to extract observables. The N_{max}-convergence of the ground-state energies obtained in these NCSM calculations at different points in the flow evolution are depicted by the colored symbols in Fig. 5. At small flow-parameters we observe the usual slow convergence of a standard NCSM calculation, with a HF basis in this case. However, with increasing flow parameter the convergence accelerates up to a point, where

Fig. 6 IM-NCSM calcula-
tions for the ground state
energies of oxygen isotopes
in comparison to the corre-
sponding NCSM results (cf.
figure 3). For odd isotopes the
IM-NCSM calculation use a
particle-attached or particle-
removed scheme starting from
even $J = 0$ reference states.
All calculations use an SRG-
evolved chiral NN+3N inter-
action with $\alpha = 0.08\,\mathrm{fm}^4$.
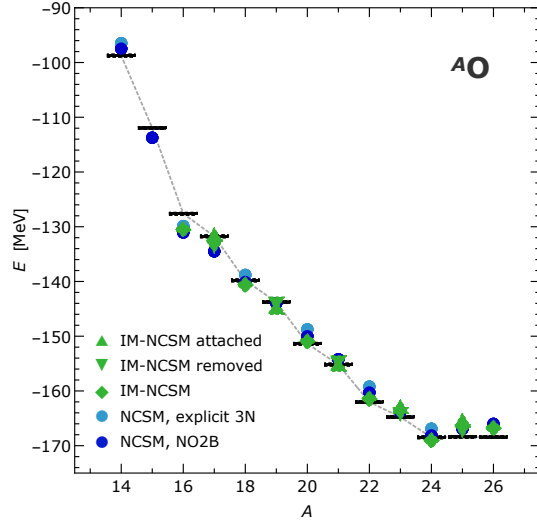
all calculations starting from $N_{\max} = 0$ provide the same result. This is the regime where the decoupling of the $N_{\max} = 0$ block is complete and, therefore, already the diagonalization within this block provides the converged ground-state energy. The converged ground-state energy is stable over a range of flow parameters, but starts to change at very large s signaling the impact of induced normal-ordered multi-particle contributions that have been truncated in the flow equations.

The combination of a NCSM calculation for the construction of the reference state, the multi-reference IM-SRG evolution for the coupling of the residual model space, and another NCSM calculation for the extraction of converged observables is very powerful. The final NCSM calculation gives access to exited states and to all relevant observables. Again, the operators for other observables, e.g. radii or electromagnetic properties, have to be transformed consistently in the IM-SRG evolution and can use a Magnus formulation of the multi-reference IM-SRG for this.

The quantification of many-body uncertainties is more difficult in the IM-NCSM than in the NCSM, since multiple truncations are involved. Nevertheless, we can construct uncertainty quantification protocols that use the dependence of observables on the main control parameters of the calculation, i.e., $N_{\max}^{\mathrm{ref}}$, $N_{\max}$, and s. To validate these protocols we can use comparisons to other ab initio methods with known uncertainties. This is illustrated in Fig. 6 for the ground-state energies of oxygen isotopes in comparison to the NCSM results discussed before. We observe a very good agreement between the two calculations. The small deviations correspond to the expected effect of the NO2B truncation on the order of 2 MeV. A similar comparison for excitation energies is presented in Fig. 7, where panel shows the IM-NCSM convergence on the left-hand-side and the NCSM convergence of the right-hand-side. For those states that are well converged we again observe good agreement, however, some states converge slowly or are sensitive to the flow-parameter of the

Fig. 7 IM-NCSM and NCSM
results for the excitation
spectra of selected carbon and
oxygen isotopes as function of
N_{max}. All calculations use an
SRG-evolved chiral NN+3N
interaction with $\alpha = 0.08\,\text{fm}^4$.
The bands shown for the IM-
NCSM results provide an
indication of the IM-SRG
flow-parameter dependence.
Modified from [85].
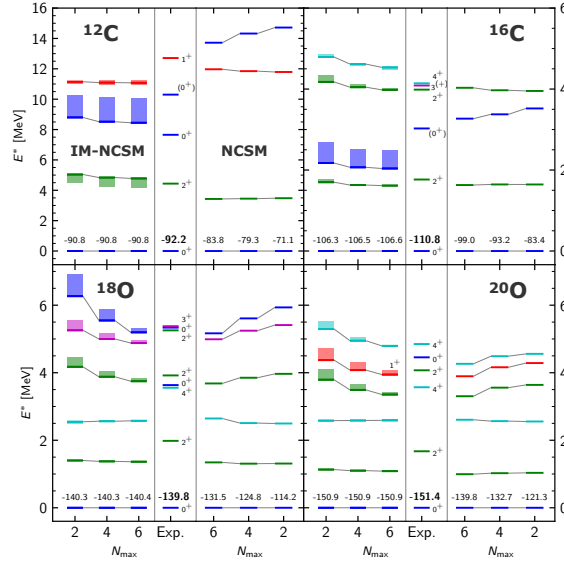
IM-SRG evolution as indicated by the shaded bands. A prominent example is the 0^+
state in ^{12}C, which has large many-body uncertainties in both, NCSM and IM-NCSM.

The IM-NCSM provides access to the same range of observables as the NCSM,
for ground excited states and for open and closed-shell systems all on the same
footing. Since N_{max}-convergence can be reached in very small model spaces, e.g.,
$N_{max} = 0$ or 2, much heavier nuclei up into the calcium region can be described with
moderate computational effort.

7 Things Left Out

Unfortunately, we could not cover all of the recent developments in ab initio nuclear
structure theory, not even in the domain of basis-expansion methods. Therefore, we
would like to provide a few references to recent review articles for filling these gaps.

In the group of decoupling methods, another prominent and important member
is coupled-cluster theory, which shares some aspects with the IM-SRG and is a
standard method in many fields of quantum many-body physics and chemistry. We
refer to [86] for an overview. Another medium-mass method used in nuclear structure
theory is based on propagator theory and known as self-consistent Green's function
method. A recent pedagogical review can be found in [87]. A big group apart from
the diagonalization and the decoupling approaches, are methods build on many-
body perturbation theory. There are many different incarnations of perturbation
theory, also in hybrid schemes combined with other ab initio methods like the
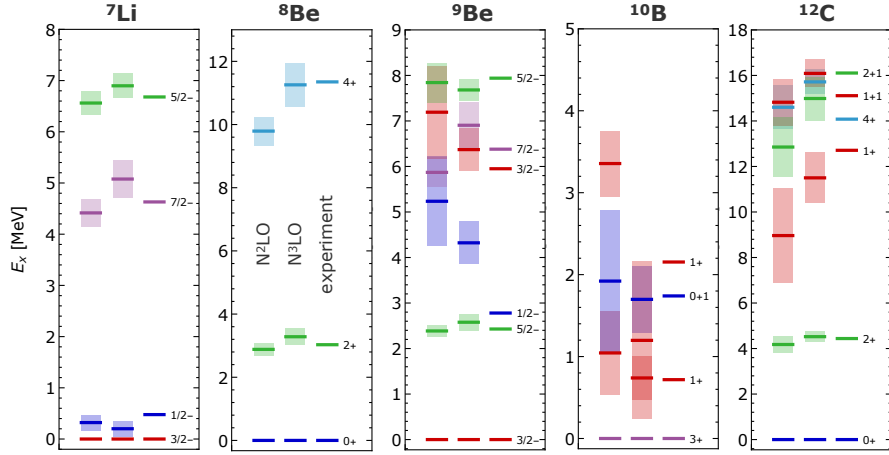NCSM. A comprehensive overview can be found in [88]. Beyond the basis-expansion

Fig. 8 NCSM calculations for the excitation spectra of p-shell nuclei using a family of nonlocal chiral NN+3N interactions up to N^3LO for cutoff $\Lambda = 500$ MeV. The excitation energies at N^2LO and N^3LO are shown with uncertainty bands extracted from the order-by-order behavior of the chiral expansion. Modified from [14].

methods, there is exciting progress on quantum Monte Carlo methods for finite nuclei, presented, e.g., in [89]. Moreover, lattice EFT methods, merging chiral EFT directly with lattice simulation techniques, have provided exciting results [90]. A nice over-all summary of the current state of ab initio methods is provided in [91].

8 The Future of Ab Initio Nuclear Structure

Instead of a summary, we provide a brief and somewhat biased outlook into the future of ab initio nuclear structure theory. We are at a point where the focus of the research work in this field is shifting. Over the past decade, the focus was on the development of ab initio frameworks that *make calculations possible*, i.e., that extend the reach of ab initio methods to heavier nuclei, open-shell systems, excited states, electromagnetic observables, etc. These developments will continue, but the focus is shifting to methodological advances that *make calculations precise and accurate*.

Discussing the *precision* of ab initio calculations requires the quantification of all the theory uncertainties that accumulate on the way from the chiral EFT formulation of the interactions to the many-body observables. Throughout the lecture we have discussed individual sources of uncertainties and ways to quantify them within the respective framework. All of this has to be propagated through the whole ab initio toolchain to the eventual observable. Illustrations of how uncertainty quantified ab initio results will look like are shown in Figs. 8, 9, and 10. We apply the full range of ab initio methods discussed in this lecture, starting from the NCSM for the
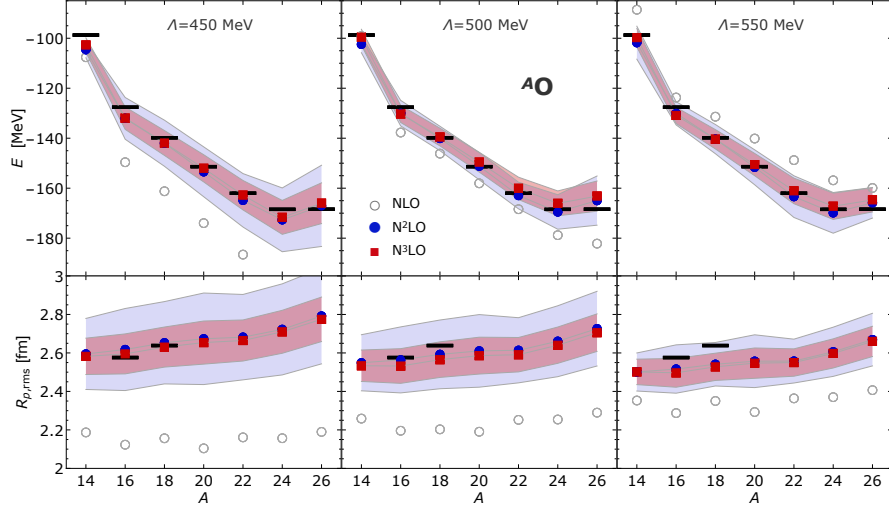
Fig. 9 IM-NCSM calculations for the ground-state energies and point-proton rms-radii of even oxygen isotopes using a family of nonlocal chiral NN+3N interactions up to N³LO for three different cutoffs. Shown are the results at NLO, N²LO, and N³LO. The results for the higher order are shown with uncertainty bands that include the chiral truncation uncertainty and the many-body uncertainties. Modified from [14].
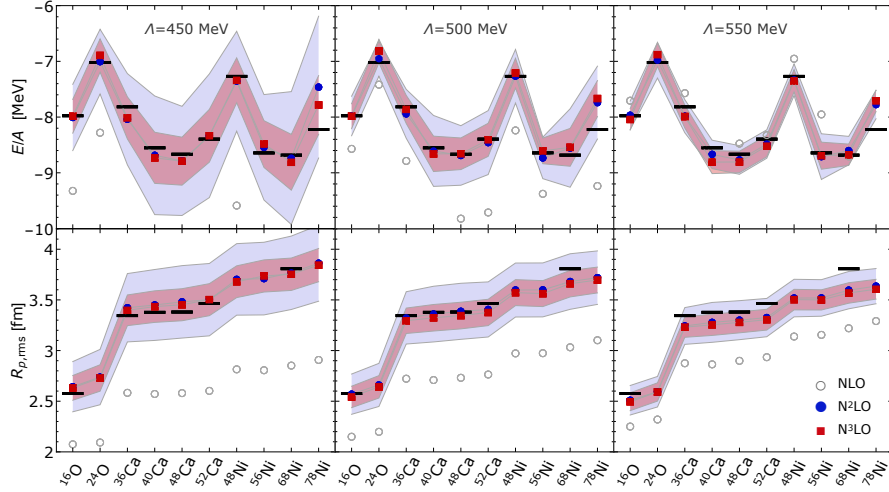

Fig. 10 IM-SRG calculations for the ground-state energies and point-proton rms-radii of closed-shell isotopes up to ^{78}Ni using a family of nonlocal chiral NN+3N interactions up to N³LO for three different cutoffs. See Fig. 9 for details. Modified from [14].

description of light nuclei and their excitation spectra in Fig. 8, via the description of beyond p-shell nuclei in the IM-NCSM in Fig. 9, to the study of medium-mass closed-shell nuclei in the IM-SRG in Fig. 10.

All calculations use a family of chiral NN+3N interactions, presented in [14], that allow for a systematic variation of the chiral order and the cutoff and, thus, enable a quantification of uncertainties due to the truncation of the chiral expansion. To this end, the many-body calculations have to be repeated for each chiral order and each cutoff, i.e., the computational cost multiplies. This is the price to pay for assessing the uncertainties related to the input interaction, an aspect that was not addressed quantitatively in past generations of ab initio calculations. The results presented in Figs. 8, 9, and 10 show that these uncertainties can be sizable, in most cases the chiral truncation uncertainties are larger than the many-body truncation uncertainties. Therefore, increasing the precision of the calculations primarily requires a reduction of the uncertainties associated with the input interactions. Work along these lines is under way with chiral EFT interactions that include conceptual improvements and higher orders [92, 93].

Assessing the *accuracy* of ab initio calculations, i.e., the agreement with experiment, once the precision is acceptable, i.e., once theory uncertainties are small enough to enable meaningful comparisons, is a next step. With the precision of the present calculations, all observables are in agreement with experiment within the estimates uncertainties. With an improved precision this can change and we might find discrepancies between theory and experiment, hinting at weak links in the chain of ab initio tools that connect nuclear structure observables to the underlying theory of the strong interaction.

References

 1. S.R. Beane, W. Detmold, K. Orginos, M.J. Savage, Prog. Part. Nucl. Phys. **66**, 1 (2011)
 2. M.J. Savage, Prog. Part. Nucl. Phys. **67**, 140 (2012)
 3. T. Inoue, Few Body Syst. **62**, 106 (2021)
 4. S. Weinberg, Phys. Lett. B **251**, 288 (1990)
 5. H. Hergert, R. Roth, Phys. Lett. B **682**, 27 (2009)
 6. U. van Kolck, Prog. Part. Nucl. Phys. **43**, 337 (1999)
 7. P.F. Bedaque, U. van Kolck, Ann. Rev. Nucl. Part. Sci. **52**, 339 (2002)
 8. E. Epelbaum, Prog. Part. Nucl. Phys. **57**, 654 (2006)
 9. E. Epelbaum, H.W. Hammer, U.G. Meissner, Rev. Mod. Phys. **81**, 1773 (2009)
10. R. Machleidt, D.R. Entem, Phys. Rept. **503**, 1 (2011)
11. E. Epelbaum, U.G. Meissner, Ann. Rev. Nucl. Part. Sci. **62**, 159 (2012)
12. H.W. Hammer, S. König, U. van Kolck, Rev. Mod. Phys. **92**, 025004 (2020)
13. Y. Nosyk, D.R. Entem, R. Machleidt, Phys. Rev. C **104**, 054001 (2021)
14. T. Hüther, K. Vobig, K. Hebeler, R. Machleidt, R. Roth, Phys. Lett. B **808**, 135651 (2020)

15. W.G. Jiang, A. Ekström, C. Forssén, G. Hagen, G.R. Jansen, T. Papenbrock, Phys. Rev. C **102**, 054301 (2020)
16. P. Reinert, H. Krebs, E. Epelbaum, Eur. Phys. J. A **54**, 86 (2018)
17. D.R. Entem, R. Machleidt, Y. Nosyk, Phys. Rev. C **96**, 024004 (2017)
18. M. Piarulli, L. Girlanda, R. Schiavilla, R. Navarro Pérez, J.E. Amaro, E. Ruiz Arriola, Phys. Rev. C **91**, 024003 (2015)
19. A. Ekström, G.R. Jansen, K.A. Wendt, G. Hagen, T. Papenbrock, B.D. Carlsson, C. Forssén, M. Hjorth-Jensen, P. Navrátil, W. Nazarewicz, Phys. Rev. C **91**, 051301 (2015)
20. E. Epelbaum, H. Krebs, U.G. Meißner, Phys. Rev. Lett. **115**, 122301 (2015)
21. A. Gezerlis, I. Tews, E. Epelbaum, M. Freunek, S. Gandolfi, K. Hebeler, A. Nogga, A. Schwenk, Phys. Rev. C **90**, 054323 (2014)
22. A. Ekström, et al., Phys. Rev. Lett. **110**, 192502 (2013)
23. D.R. Entem, R. Machleidt, Phys. Rev. C **68**, 041001 (2003)
24. U. van Kolck, Front. in Phys. **8**, 79 (2020)
25. E. Epelbaum, H. Krebs, P. Reinert, Front. in Phys. **8**, 98 (2020)
26. B.D. Carlsson, A. Ekström, C. Forssén, D.F. Strömberg, G.R. Jansen, O. Lilja, M. Lindby, B.A. Mattsson, K.A. Wendt, Phys. Rev. X **6**, 011019 (2016)
27. E. Epelbaum, H. Krebs, U.G. Meißner, Eur. Phys. J. A **51**, 53 (2015)
28. S. Binder, et al., Phys. Rev. C **93**, 044002 (2016)
29. S. Binder, et al., Phys. Rev. C **98**, 014002 (2018)
30. R.J. Furnstahl, N. Klco, D.R. Phillips, S. Wesolowski, Phys. Rev. C **92**, 024005 (2015)
31. J.A. Melendez, S. Wesolowski, R.J. Furnstahl, Phys. Rev. C **96**, 024003 (2017)
32. S. Wesolowski, R.J. Furnstahl, J.A. Melendez, D.R. Phillips, J. Phys. G **46**, 045102 (2019)
33. J.A. Melendez, R.J. Furnstahl, D.R. Phillips, M.T. Pratola, S. Wesolowski, Phys. Rev. C **100**, 044001 (2019)
34. A. Ekström, G. Hagen, Phys. Rev. Lett. **123**, 252501 (2019)
35. S. Okubo, Prog. Theor. Phys. **12**, 603 (1954)
36. K. Suzuki, S.Y. Lee, Prog. Theor. Phys. **64**, 2091 (1980)
37. H. Feldmeier, T. Neff, R. Roth, J. Schnack, Nucl. Phys. A **632**, 61 (1998)
38. H. Hergert, R. Roth, Phys. Rev. C **75**, 051001 (2007)
39. R. Roth, T. Neff, H. Feldmeier, Prog. Part. Nucl. Phys. **65**, 50 (2010)
40. F. Wegner, Ann. Phys. (Leipzig) **3**, 77 (1994)
41. F.J. Wegner, Phys. Rep. **348**, 77 (2001)
42. S.D. Glazek, K.G. Wilson, Phys. Rev. D **48**, 5863 (1993)
43. S.K. Bogner, R.J. Furnstahl, R.J. Perry, Phys. Rev. C **75**, 061001 (2007)
44. S.K. Bogner, R.J. Furnstahl, A. Schwenk, Prog. Part. Nucl. Phys. **65**, 94 (2010)
45. R. Roth, J. Langhammer, A. Calci, S. Binder, P. Navratil, Phys. Rev. Lett. **107**, 072501 (2011)
46. R. Wirth, R. Roth, Phys. Rev. C **100**, 044313 (2019)
47. W. Magnus, Commun. Pure Appl. Math. **7**, 649 (1954)
48. T.D. Morris, N. Parzuchowski, S.K. Bogner, Phys. Rev. C **92**, 034331 (2015)
49. S. Szpigel, R.J. Perry, *Quantum Field Theory - A 20th Century Profile* (Hindustan Book Agency, 2000), chap. The Similarity renormalization group, pp. 59–81
50. R. Roth, A. Calci, J. Langhammer, S. Binder, Phys. Rev. C **90**, 024325 (2014)
51. R. Roth, S. Binder, K. Vobig, A. Calci, J. Langhammer, P. Navratil, Phys. Rev. Lett. **109**, 052501 (2012)
52. I. Talmi, Helv. Phys. Acta **25**, 185 (1952)
53. M. Moshinsky, Nucl. Phys. **13**, 104 (1959)
54. M. Moshinsky, Y.F. Smirnov, *The harmonic oscillator in modern physics* (Harwood academic Publishers, Amsterdam, 1996)
55. G.P. Kamuntavicius, R.K. Kalinauskas, B.R. Barrett, S. Mickevicius, D. Germanas, Nucl. Phys. A **695**, 191 (2001)
56. P. Ring, P. Schuck, *The nuclear many-body problem* (Springer-Verlag, New York, 1980)
57. J. Suhonen, *From Nucleons to Nucleus: Concepts of Microscopic Nuclear Theory*. Theoretical and Mathematical Physics (Springer, Berlin, Germany, 2007)

58. R. Roth, P. Papakonstantinou, N. Paar, H. Hergert, T. Neff, H. Feldmeier, Phys. Rev. C **73**, 044312 (2006)
59. C. Constantinou, M.A. Caprio, J.P. Vary, P. Maris, Nucl. Sci. Tech. **28**, 179 (2017)
60. A. Tichai, J. Müller, K. Vobig, R. Roth, Phys. Rev. C **99**, 034321 (2019)
61. I. Shavitt, R.J. Bartlett, *Many-Body Methods in Chemistry and Physics: MBPT and Coupled-Cluster Theory*. Cambridge Molecular Science (Cambridge University Press, 2009)
62. S. Binder, J. Langhammer, A. Calci, P. Navratil, R. Roth, Phys. Rev. C **87**, 021303 (2013)
63. S. Binder, J. Langhammer, A. Calci, R. Roth, Phys. Lett. B **736**, 119 (2014)
64. W. Kutzelnigg, D. Mukherjee, The Journal of Chemical Physics **107**, 432 (1997)
65. D. Mukherjee, Chemical Physics Letters **274**, 561 (1997)
66. L. Kong, M. Nooijen, D. Mukherjee, The Journal of Chemical Physics **132**, 234107 (2010)
67. E. Gebrerufael, A. Calci, R. Roth, Phys. Rev. C **93**, 031301 (2016)
68. B.R. Barrett, P. Navratil, J.P. Vary, Prog. Part. Nucl. Phys. **69**, 131 (2013)
69. P. Navratil, S. Quaglioni, I. Stetcu, B.R. Barrett, J. Phys. G **36**, 083101 (2009)
70. R. Roth, P. Navratil, Phys. Rev. Lett. **99**, 092501 (2007)
71. R. Roth, Phys. Rev. C **79**, 064324 (2009)
72. C. Stumpf, J. Braun, R. Roth, Phys. Rev. C **93**, 021301 (2016)
73. P. Navratil, G.P. Kamuntavicius, B.R. Barrett, Phys. Rev. C **61**, 044001 (2000)
74. C. Forssén, B.D. Carlsson, H.T. Johansson, D. Sääf, A. Bansal, G. Hagen, T. Papenbrock, Phys. Rev. C **97**, 034328 (2018)
75. M. Shao, H.M. Aktulga, C. Yang, E.G. Ng, P. Maris, J.P. Vary, Computer Physics Communications **222**, 1 (2018)
76. K. Tsukiyama, S.K. Bogner, A. Schwenk, Phys. Rev. Lett. **106**, 222502 (2011)
77. H. Hergert, S.K. Bogner, S. Binder, A. Calci, J. Langhammer, R. Roth, A. Schwenk, Phys. Rev. C **87**, 034307 (2013)
78. H. Hergert, S.K. Bogner, T.D. Morris, A. Schwenk, K. Tsukiyama, Phys. Rept. **621**, 165 (2016)
79. H. Hergert, S.K. Bogner, J.G. Lietz, T.D. Morris, S. Novario, N.M. Parzuchowski, F. Yuan, Lect. Notes Phys. **936**, 477 (2017)
80. H. Hergert, Phys. Scripta **92**, 023002 (2017)
81. K. Tsukiyama, S.K. Bogner, A. Schwenk, Phys. Rev. C **85**, 061304 (2012)
82. S.R. Stroberg, A. Calci, H. Hergert, J.D. Holt, S.K. Bogner, R. Roth, A. Schwenk, Phys. Rev. Lett. **118**, 032502 (2017)
83. H. Hergert, S. Binder, A. Calci, J. Langhammer, R. Roth, Phys. Rev. Lett. **110**, 242501 (2013)
84. H. Hergert, S.K. Bogner, T.D. Morris, S. Binder, A. Calci, J. Langhammer, R. Roth, Phys. Rev. C **90**, 041302 (2014)
85. E. Gebrerufael, K. Vobig, H. Hergert, R. Roth, Phys. Rev. Lett. **118**, 152503 (2017)
86. G. Hagen, T. Papenbrock, M. Hjorth-Jensen, D.J. Dean, Rept. Prog. Phys. **77**, 096302 (2014)
87. V. Somà, Front. in Phys. **8**, 340 (2020)
88. A. Tichai, R. Roth, T. Duguet, Front. in Phys. **8**, 164 (2020)
89. S. Gandolfi, D. Lonardoni, A. Lovato, M. Piarulli, Front. in Phys. **8**, 117 (2020)
90. T.A. Lähde, U.G. Meißner, *Nuclear Lattice Effective Field Theory: An introduction*, vol. 957 (Springer, 2019)
91. H. Hergert, Front. in Phys. **8**, 379 (2020)
92. E. Epelbaum, et al., Phys. Rev. C **99**, 024313 (2019)
93. P. Maris, et al., Phys. Rev. C **103**, 054001 (2021)